Ultrasound in Med. & Biol., Vol. 42, No. 5, pp. 1145–1166, 2016

0301-5629/$ - see front matter

http://dx.doi.org/10.1016/j.ultrasmedbio.2015.12.011

● *Original Contribution*

ACOUSTIC CLUSTER THERAPY: *IN VITRO* AND *EX VIVO* MEASUREMENT OF ACTIVATED BUBBLE SIZE DISTRIBUTION AND TEMPORAL DYNAMICS

Andrew John Healey,* Per Christian Sontum,* Svein Kvåle,* Morten Eriksen,† Ragnar Bendiksen,‡ Audun Tornes,§ and Jonny Østensen¶

*Phoenix Solutions AS, Oslo, Norway; †University of Oslo, Oslo, Norway; ‡Medistim ASA, Oslo, Norway; §Ultimovacs AS, Oslo, Norway; and ¶Inven2 AS, Oslo, Norway

(*Received* 4 *June* 2015; *revised* 7 *December* 2015; *in final form* 14 *December* 2015)

Abstract—Acoustic cluster technology (ACT) is a two-component, microparticle formulation platform being developed for ultrasound-mediated drug delivery. Sonazoid microbubbles, which have a negative surface charge, are mixed with micron-sized perfluoromethylcyclopentane droplets stabilized with a positively charged surface membrane to form microbubble/microdroplet clusters. On exposure to ultrasound, the oil undergoes a phase change to the gaseous state, generating 20- to 40-μm ACT bubbles. An acoustic transmission technique is used to measure absorption and velocity dispersion of the ACT bubbles. An inversion technique computes bubble size population with temporal resolution of seconds. Bubble populations are measured both *in vitro* and *in vivo* after activation within the cardiac chambers of a dog model, with catheter-based flow through an extracorporeal measurement flow chamber. Volume-weighted mean diameter in arterial blood after activation in the left ventricle was 22 μm, with no bubbles >44 μm in diameter. After intravenous administration, 24.4% of the oil is activated in the cardiac chambers. (E-mail: Andrew.healey@phoenixsolutions.no) © **2016 World Federation for Ultrasound in Medicine & Biology.**

Key Words: **Acoustic cluster therapy, *In vitro* bubble sizing, *Ex vivo* bubble sizing, *In vivo* bubble sizing, Microbubbles, Droplet vaporization, Ultrasound contrast agent, Myocardial perfusion imaging.**

INTRODUCTION

Acoustic cluster technology (ACT) can be considered to belong to the class of technologies based on acoustic droplet vaporization (ADV), a term first used in the literature in 2000 (Kripfgans et al. 2000). Liquid droplets of micron and submicron diameter (also referred to as phase shift emulsions) are provided an energy stimulus (ultrasound for "acoustic" droplet vaporization) to change phase from liquid to gas-forming microbubbles. ADV has been extensively researched for albumin-coated micrometer-sized dodecafluoropentane droplets by the group at the University of Michigan, among others. For a historical review, see Sheeran and Dayton (2012).

Several patents were granted related to ADV in the late 1990s. Apfel (1998) describes dispersions of superheated droplets (droplet liquid has a boiling point below body temperature at atmospheric pressure) of immiscible liquids for infusion, which are vaporizable by ionizing radiation or ultrasound. Applications described include diagnostic contrast agents, drug delivery and embolization. Østensen et al. (1998) describe a similar concept in which micron-sized droplets are mixed with stabilized microbubbles that significantly reduce the ultrasound energy required to vaporize the droplets and allow use of droplets that are not necessarily superheated. Eriksen and Tolleshaug (1999) reported that the efficacy of the concept (described in Østensen et al. 1998) can be substantially enhanced if the emulsion droplets and microbubbles have affinity for each other. These two patents exploit the deposit nature of the vaporized bubbles for perfusion imaging, for bubble sizes sufficient to lodge in the microvasculature. The gold standard for perfusion measurements in tissue is injection of labeled, solid microspheres that are trapped in capillaries because of their size (deposit tracer). The deposition of microspheres will be proportional to flow in tissue if certain conditions are met (Domenech et al. 1969). Vaporized bubbles that are large enough to trap in the capillary bed also behave as a deposit tracer; the number of bubbles deposited in

Address correspondence to: Andrew John Healey, CSO, Phoenix Solutions AS, PO Box 4741, N-0421 Oslo, Norway. E-mail: Andrew.healey@phoenixsolutions.no

tissue is related to tissue perfusion. The gold standard microsphere technique is not suitable for imaging for two main reasons. Solid microspheres do not pass the lung capillaries and must therefore be injected via arterial catheters. The residence time may also be unacceptably long. The use of vaporized bubbles of sufficient size overcomes these two limitations. The liquid droplets have been designed to grow in size when activated by ultrasound after they have passed the pulmonary capillaries and can therefore be administered intravenously. The bubbles so generated contain a gas that dissolves in tissue after deposition and have a residence time of minutes. Thus, the additional backscatter signal provided by the bubbles deposited in tissue is related to tissue perfusion.

Smaller droplets (submicron) will produce smaller bubbles that may not have the same deposit tracer properties. Nanodroplets have the potential to leave the vasculature, for example, by the enhanced permeability and retention effect (Iyer et al. 2006), prior to vaporization and be vaporized in the tissue compartment (Sheeran and Dayton 2012).

Bubbles produced by *in vivo* vaporization of liquid droplets have been proposed for a plethora of applications (for recent reviews, see Lin and Pitt 2013; Rapoport 2012; Sheeran and Dayton 2012) embracing their ultrasound imaging properties including perfusion imaging; embolization; phase aberration correction; thrombolysis; influence on high-intensity focused ultrasound therapy; and drug delivery.

The ACT concept is a two-component microparticle system composed of stabilized microbubbles with a negative surface charge mixed with stabilized perfluoromethylcyclopentane (PFMCP) microdroplets with a positive surface charge (Sontum et al. 2015b). On mixing, small 2- to 8-μm particle clusters are formed by electrostatic attraction. When injected into the bloodstream and exposed to medical ultrasound fields, the microbubble transfers energy to the microdroplet and acts as a vaporization "seed," initiating vaporization of the oil droplet. The presence of the microbubble in the cluster makes the vaporization process occur at much lower acoustic power than it would in its absence (Eriksen and Tolleshaug 1999; Lo et al. 2007; Østensen et al. 1998). The initial vaporization step is rapid (microsecond time scale for ADV droplets without the microbubble present [Doinikov et al. 2014; Shpak et al. 2013, 2014; Wong et al. 2011]) and results in a vapor bubble approximately five times the initial droplet diameter (Kripfgans et al. 2000). Inward diffusion of blood gases and water vapor results in continued bubble growth to reach a maximum diameter. Gas under saturation in blood as a result of O_2 metabolism, surface tension and blood pressure promotes diffusion of gases out of the bubbles and subsequent shrinkage (Van Liew and Burkard 1995a). A low-solubility oil is employed to extend the lifetime of the activated ACT bubble.

The average diameter of lung capillaries has been reported to be approximately 7 μm, with approximately 95% being larger than 4 μm (Hogg 1987). To ensure free-flowing properties and passage through the capillary bed after intravenous administration, medical ultrasound contrast agents are therefore typically <4 μm in mean diameter (Sontum 2008). In dogs, experiments have indicated that bubbles <11 μm are required for lung passage (Butler and Hills 1979). ACT bubbles ≥ 12 μm in diameter will hence be expected to lodge and deposit in the capillary bed, transiently stopping blood flow until they dissolve and become small enough to dislodge, re-condense or dissolve completely. The 20- to 30-μm average diameters imply that they are likely to lodge at the capillary level. Currently, ACT technology is being developed for ultrasound-mediated drug delivery applications as a theranostic agent. For recent reviews of related approaches, see Castle et al. (2013) and Wood and Sehgal (2015).

To enable formulation design and to elucidate attributes and mechanisms, there was an obvious need for experimental methods capable of sizing the activated bubbles *in vitro* and *in vivo*, to track their kinetics and to measure the efficiency of the activation process (*i.e.*, the fraction of injected oil that vaporizes in both the *in vitro* and *in vivo* environments). Measuring bubble size populations in multiphasic media is an important problem in a plethora of applications including industry (nuclear reactors), medicine (decompression sickness), biology and oceanography. A method was required that could size an entire bubble population *in vitro* at controlled concentrations and environmental settings similar to those *in vivo* with a temporal resolution of seconds. The method was also required to operate in whole blood in an extracorporeal flow circuit, to size bubble populations after *in vivo* activation. The activated ACT bubbles are mostly devoid of a stabilizing shell or membrane (except for the remnants of the particle shells in the original cluster). In larger vessels they may be considered as "free" bubbles, which possess relatively "sharp" acoustic resonances in the linear regime. This is due to the increase in Q factor of the bubble system without a shell and the increase in Q factor with bubble size. This allows for use of the acoustic attenuation properties of a bubble population along with a model of bubble resonance to invert the linear attenuation data to recover bubble size. This technique has been used in the sonar literature to size bubbles in the upper ocean (Vagle and Farmer 1998) and is employed in a commercially available bubble-sizing instrument (Wu and Chahine 2010). This quantitative approach also has the advantage of operating well in whole blood and is insensitive to the

non-gaseous particles present. Simultaneous measurement of the entire bubble population size range requires measurement covering the whole range of resonance frequencies in the bubble population. This may be achieved by using a broadband acoustic transmission technique. For an artifact-free measurement it is important to excite the bubble population in the linear range. Studies have indicated that a non-linear response to ultrasound exposure has a very low threshold for many medical ultrasound contrast agents, and a predominantly linear response is achieved only for excitation pressure amplitudes <30 kPa (Chatterjee et al. 2005; Qin et al. 2009).

METHODS

Materials

The microbubbles used were the commercially available ultrasound contrast agent Sonazoid (GE Healthcare, Oslo, Norway), which, on reconstitution, contains 8 μL bubble gas volume per milliliter (ca. 1.1×10^9 microbubbles/mL), with a volume-weighted median diameter of 2.6 μm (Sontum 2008). The microdroplets (emulsion component) consisted of perfluoromethylcyclopentane stabilized with a distearoylphosphatidylcholine phospholipid membrane containing 3% stearylamine to produce the positive surface charge (Sontum et al. 2015b), with 3.2 μL PFMCP microdroplets/mL (approx. 0.6×10^9 microdroplets/mL) and a volume-weighted median droplet diameter of 2.8 μm. The ACT compound for injection (the drug product) was prepared by reconstituting a vial of Sonazoid with 2 mL of the emulsion component.

Models of size dynamics

There are several mathematical models in the literature that are applicable to the activated ACT bubble size and temporal kinetics (Burkard and Van Liew 1994; Kabalnov et al. 1998; Kausik et al. 2009; Van Liew and Burkard 1995a, 1995b). The specifics of the model and parameter values for calculations used in this article are given in the Appendix.

Coulter counting

Coulter analysis of the microdroplet component was performed using a Coulter Multisizer III (Beckman Coulter, Brea, CA, USA) instrument set up with a 50-μm aperture and a measuring range of 1 to 30 μm. A suitable aliquot of the sample was dispersed and homogenized in Isoton II electrolyte (phosphate-buffered saline; Beckman Coulter) prior to analysis. Responses were number and volume concentration and number and volume size distributions.

Flow particle image analysis

Flow particle image analysis is a fully automated microscopy and image analysis technique. A suitable aliquot of the ACT compound is dispersed in particle-free Isoton II and homogenized. A known portion of the diluted sample is then drawn through the measuring cell in the instrument, where a fixed set of micrographs are taken by a charge-coupled device camera with a stroboscopic light source. The particles in each frame are automatically isolated and analyzed by the image analysis software, and a variety of morphologic parameters are calculated for each particle, as is the total particle concentration. The instrument provides a representative selection of micrographs for different size classes. <5, 5–10, 10–20 and 20–40 μm, together with concentration observed in each class. For the reported analyses, a Sysmex 2100 flow particle image analysis instrument (Malvern Instruments, Malvern, UK) set up with a high-power field (20× magnification) and measuring range of 0.7 to 40 μm was used. The cluster concentration in each size range was reported as primary parameters for evaluation. Analyses were also performed using 5% human serum albumin (HSA, CSL Behring, Breda, Netherlands) as diluent.

Activated ACT bubble sizing in vitro

An acoustic transmission technique was used to measure the size distribution dynamics of the ACT bubble population after activation. Figure 1 is a schematic of the measurement system. A low-frequency (250-kHz center frequency, Olympus Videoscan, part V1012, Waltham, MA, USA) broadband pulse is directed through a sample cell, is reflected from a steel plate (approx. 25 cm from the low-frequency transducer), propagates back through the sample and is received by the same transducer. The sample cell has a volume of 236.28 cm^3. The cell is closed (*i.e.*, contains no head space) so that it may be kept at a controlled gas saturation. Stirring is incorporated to ensure adequate mixing. Mylar membranes are used to provide acoustically transparent windows. The bandwidth of the low-frequency pulse is

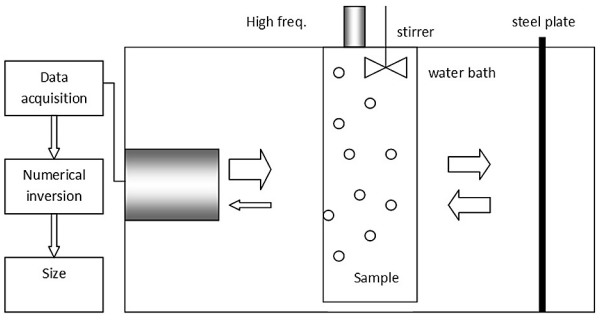

Fig. 1. Schematic of *in vitro* sonometry system.

able to cover a bubble size range from 4 to 80 μm in diameter (76 kHz to 1.36 MHz). The third and fifth harmonics of the transducer are used to cover this frequency range. There are minima in the transmitted pulse spectra around 0.5 MHz (second harmonic) and 1 MHz (fourth harmonic). The two measurements (one to either side of 0.5 MHz, corresponding to bubble resonance frequencies of 10- and 12-μm bubbles) have a low signal-to-noise ratio and are replaced with cubic spline interpolation data from the surrounding measurement points. The peak negative pressure of the low-frequency pulse was measured to be 14 kPa, measured with a 0.5-mm membrane hydrophone (GEC Marconi, Chelmsford, Essex, UK), with National Physics Laboratory calibration extended to 0.25 MHz. The low-frequency source does not activate the ACT clusters. Activation is provided by a clinical scanner (ATL [Philips] HDI 5000, Bothell, WA, USA), with a P3-2 probe, B-mode imaging, single focus at 10-cm image depth (center of *in vitro* cell) and 21-Hz frame rate. To quantify the effect of the displayed scanner mechanical index (MI) setting on the amount of activation produced *in vitro*, experiments were repeated at all output settings available on the scanner with this probe (ranging from MI 0.0 to 1.0).

The measurement system is placed in a water bath at 37°C to mimic body temperature. The gas saturation *in vivo* (approximately 98 kPa in arterial blood and 90 kPa in venous blood), coupled with systemic overpressure (13.3 kPa average arterial pressure), provides an *in vivo* gas saturation environment of approximately 85% (Van Liew and Burkard 1995a). The sample cell contains Isoton II at 85% gas (air) saturation (37°C). This is achieved by storing the Isoton II at 44°C for at least 48 h prior to transfer to the sample cell, to allow gas saturation to be reached at this temperature. The stirred sample cell was filled and left to stand for a few minutes until thermal equilibrium at 37°C was reached. Analyses were also performed using 5% HSA instead of Isoton II, also at 85% air saturation.

Two hundred consecutive radiofrequency A-line signals are recorded at 10- MHz sampling frequency, 12-bit resolution and comprise one measurement data set (ADC model, National Instruments PCI 6115, Austin, TX, USA). The pulse repetition frequency (PRF) of the transmission transducer is set at 200 Hz, and thus, 1 s is required for data capture. The transmission transducer is activated with a Panametrics 5800 Pulser/Receiver (Waltham, MA, USA) with the following settings: mode: pulser receiver; PRF: 200 Hz; energy: 12.5 μJ; damping: 50 Ohm; high-pass filter: 1 kHz; low-pass filter: 5 MHz; input attenuation: 0.0 dB; output attenuation: 0.0 dB; gain: 40 dB. Ninety-one consecutive data sets were recorded with an interval of 3 s between measurements.

The first two measurement sets are recorded with no product added and serve as a reference data set in the absence of the bubbles. After measurement 2, 3.5 μL of the ACT formulation is added to the sample cell and homogenized. Two more measurements are recorded with the product added, but with no acoustic output from the scanner transducer used for activation (data sets 3 and 4). Activation is then initiated prior to the recording of data set 5 and maintained for 30 s. The log spectral difference method, using measurements 1 and 2 as the reference (bubble-free) data, is used to determine the additional attenuation resulting from the bubble population.

Numerical inversion

Details of the bubble model used are given in the Appendix. Inverting the measured acoustic attenuation data to yield size distribution information is based on a simple finite-element solution as proposed by Commander and McDonald (1991). The resulting equation relating attenuation to size distribution is the Fredholm integral equation:

$$\alpha(f) = \int_{a_{\min}}^{a_{\max}} \sigma_e(f,a)\Psi(a)da \tag{1}$$

where $\alpha(f)$ is the measured frequency-dependent acoustic attenuation, $\Psi(a)$ is the unknown bubble number density function and $\sigma_e(f,a)$ is the bubble extinction cross section as a function of frequency and bubble radius. $\Psi(a)$ is expanded with a finite sum of basic functions, in this case linear B splines. Suitable quadrature is then employed in conjunction with a weighted residual method (collocation) to generate a linear system of equations for the coefficients of the B splines. $\Psi(a)$ is thus approximated via

$$\Psi(a) = \sum_{j=1}^{N} \Psi_j B_j(a) \tag{2}$$

where Ψ_j takes the value of the function Ψ at the value a_j, and $B_j(a)$ is the jth linear B spline. The linear system of equations below is then arrived at directly by substitution:

$$\alpha(f_i) = \sum_{j=1}^{N} K_{ij}\Psi_j \tag{3}$$

Here,

$$K_{ij} = \int_{a_{\max}}^{a_{\min}} \sigma_e(f_i,a)B_j(a)da \tag{4}$$

This integral is computed with an appropriate quadrature scheme. The system is expressed in matrix notation as

$$\begin{pmatrix} \alpha_1 \\ \alpha_2 \\ \vdots \\ \alpha_N \end{pmatrix} = \begin{pmatrix} K_{11} & K_{12} & \cdots & K_{1N} \\ K_{21} & K_{22} & \cdots & K_{2N} \\ \vdots & \vdots & & \vdots \\ K_{N1} & K_{N2} & \cdots & K_{NN} \end{pmatrix} \begin{pmatrix} \Psi_1 \\ \Psi_2 \\ \vdots \\ \Psi_N \end{pmatrix} \quad (5)$$

As the linear system is ill-conditioned in the sense of Hadamard, choosing the B spline knot locations to coincide with the resonance radius frequencies in the attenuation data can improve the condition of the matrix and is employed here. Commander and McDonald (1991) had to make use of a regularization procedure based on restricting the solution to a minimum curvature constraint to stabilize the resulting system. Other stabilization systems have also been explored for this problem (Duraiswami 1993). However, for the attenuation data measured in the *in vitro* system described previously, the range of bubble sizes and data signal-to-noise ratios is such that these techniques are typically not required. The system of equations is adequately solved by the standard least-squares methodology with an additional non-negativity constraint, that is,

$$\min_{\Psi} \frac{1}{2}\|K\Psi - \alpha\|_2^2 \text{such that } \Psi \geq 0 \quad (6)$$

The details of the algorithm used can be found in Lawson and Hanson (1974). The non-negativity constraint is incorporated for obvious physical reasons (there cannot be a negative number of bubbles per unit volume).

From the acoustic measurements, acoustic attenuation and velocity as a function of frequency may both be calculated. Only attenuation data are used to calculate the bubble distribution; the velocity data can be used as the basis of an independent check of the estimated bubble size distribution.

Inversion quality metric

The velocity of a bubbly liquid is highly dispersive around the resonance frequency. This phenomenon may be used to derive a "quality" metric to quantitatively infer the accuracy or confidence of the estimated bubble distribution (Vagle and Farmer 1998). The summation (over the B spline knot locations) of the discrepancy between the measured sound speed and the sound speed calculated from the estimated bubble population, weighted so as to emphasize the part of the bubble size spectrum contributing most to the volume fraction, is used to define a quality metric, Q_m,

$$Q_m = 1 - \frac{\left| \sum_j |\Delta c_j| \beta_j \right|^2}{\sum_j |dc'_j| \beta_j \times \sum_j |dc''_j| \beta_j} \quad (7)$$

where β_j is the volume fraction at the jth B spline knot location, dc'_j is the sound speed anomaly (the difference between the sound speed with and without the bubble cloud present) calculated from the bubble distribution derived through the measured attenuation, dc''_j is the sound speed anomaly calculated from the measurement data and Δc_j is the difference between the two. A perfect correspondence between the measured sound speed anomaly and that calculated from the derived bubble distribution gives a Q_m value of 1 (when the second term on the right-hand side of eqn [7] is 0). Thus, Q_m provides a quantitative parameter defining the quality of the inversion that is derived from "independent" data to that of data used for the inversion.

Numerical inversion performance estimates

Uncertainty estimates for the inversion procedure were determined around the "operating point" of the instrument reported in this article using the following (computer simulation) method. This accounts for the acoustic pulses used in the measurement, the signal-to-noise ratio level of the measurement data, the bubble size distribution and the bubble concentration measured. It assumes that the bubble models are correct. The acoustic pulse used to size the bubble population was measured in the absence of bubbles in the extracorporeal flow circuit used for the *in vivo* activation experiments. The average of 2000 pulses was used to represent a "noise-free" signal. For the in vivo activation experiments, 200 pulses were averaged. The noise content of the 200 pulse averages was measured from a section of the radiofrequency data before the arrival of the ultrasound pulse. The power in this noise term was measured. The noise is assumed to be a normally distributed additive independent random process.

The simulated bubble distribution has a Gaussian volume-weighted distribution with a mean of 22 μm and a full width half-maximum ranging from 10 to 25 μm. The choice of Gaussian distribution is based on the parent emulsion distribution. Note that the recovered distribution is in the range of 4–80 μm, and the Gaussian distribution is accordingly truncated to this range.

For each simulated Gaussian distribution the following procedure is applied.

- The measured "noise-free" pulse is propagated through the measurement cell *in silico*, using the bubble model, simulated size distribution, concentration and sample cell path length.
- Noise is then added to the "noise-free" pulse at the noise level of the instrument and also to the pulse after simulated propagation through the bubble cloud. These then form the reference and bubble population measurements as input to the bubble size distribution inversion procedure.

- The inversion procedure is performed.
- This is repeated for 10,000 runs.

To check for bias and error bounds for the inversion procedure, the median and 2.5% and 97.5% quantiles were calculated for the recovered bubble distribution parameters and compared with simulation input.

Activated ACT bubble sizing ex vivo *extracorporeal measurement chamber*

A measurement chamber was constructed to measure bubble population size dynamics in an *ex vivo* extracorporeal flow circuit after activation of ACT *in vivo* in the cardiac chambers in a dog model. Figure 2 is a schematic of the extracorporeal circuit. It uses the same transmit transducer and driving electronics as the *in vitro* measurement system, but employs a 100-μm-thick polyvinylidene difluoride film as the receiver. Two hundred pulses were generated at 400-Hz PRF for a 0.5-s measurement time and repeated every 3 s for a total of 91 measurements. There are two sets of three-way valves on each of the connections to the test chamber. This is to allow for ease of priming and subsequent connection of the flow lines to and from the animal. The test cell chamber is first primed with saline solution at 85% gas saturation to avoid bubble formation. The primed chamber is placed in a water bath kept at a constant 37°C for at least 30 min prior to use to allow for thermal equilibrium.

uniform concentration, C, within the cell. The initial concentration at $t = 0$ in the cell is $C = 0$. Consider a small volume, ΔV, which enters the cell after passage through the inlet tube with transit time t_t, at concentration $c_i e^{-\alpha_1 t - \alpha_2 t_t}$. The concentration of this volume ΔV at time $t + \Delta t$ will be

$$e^{-\alpha_2 t_t}\frac{c_i}{\Delta t}\int_t^{t+\Delta t} e^{-\alpha_1 t'} e^{-\alpha_2 (t-t'+\Delta t)} dt' \tag{8}$$

Here α_1 is the time constant associated with the bolus (modeled as an exponential decay). α_2 is the time constant associated with the lifetime of the ACT bubble population (modeled as an exponential decay) and t_t is the transit time through the arterial catheter to the measurement chamber. A commensurate volume exits the cell. The original concentration within the cell is now $Ce^{-\alpha_2 \Delta t}$. Thus, the overall change in concentration in the cell is

$$\begin{aligned}\Delta C &= \frac{(V_0-\Delta V)Ce^{-\alpha_2\Delta t} + \Delta V e^{-\alpha_2 t_t}\frac{c_i}{\Delta t}\int_t^{t+\Delta t} e^{-\alpha_1 t'} e^{-\alpha_2(t-t'+\Delta t)} dt'}{V_0} - C \\ &= C\left(e^{-\alpha_2\Delta t}-1\right) - \frac{\Delta V}{V_0} C e^{-\alpha_2\Delta t} + \frac{\Delta V}{V_0} c_i e^{-\alpha_2 t_t} e^{-t\alpha_1-\alpha_2\Delta t}\left[\frac{1}{\Delta t(\alpha_1-\alpha_2)} - \frac{e^{\Delta t(-\alpha_1+\alpha_2)}}{\Delta t(\alpha_1-\alpha_2)}\right]\end{aligned} \tag{9}$$

$\dot{Q}$ is the rate of flow through the cell. Flow is pulsatile with heartbeat, but as the measurement time averages over the cardiac cycle, $\dot{Q}$ is modeled as constant.Noting that

$$\Delta V = \dot{Q}\Delta t \tag{10}$$

we express eqn (9) as

$$\Delta C = C\left(e^{-\alpha_2\Delta t}-1\right) - \frac{\dot{Q}\Delta t}{V_0} c e^{-\alpha_2\Delta t} + \frac{\dot{Q}\Delta t}{V_0} c_i e^{-\alpha_2 t_t} e^{-t\alpha_1-\alpha_2\Delta t}\left[\frac{1}{\Delta t(\alpha_1-\alpha_2)} - \frac{e^{\Delta t(-\alpha_1+\alpha_2)}}{\Delta t(\alpha_1-\alpha_2)}\right] \tag{11}$$

Simple model for bubble volume estimation from ex vivo *cell measurements*

A simple model was derived to estimate the peak concentration in the measurement cell, as a function of flow rate into the cell and the ACT bubble half-life and bolus half-life. We have a measurement cell of volume V_0 with an inlet port and an outlet port. The compartment is assumed to be well stirred, with

By dividing each side by Δt, using some expansions and taking the limit as $\Delta t \to 0$, we have a first-order ordinary differential equation

$$\frac{dC}{dt} = -C\alpha_2 - \frac{\dot{Q}}{V_0} C + \frac{\dot{Q}}{V_0} c_i e^{-\alpha_2 t_t - \alpha_1 t} \tag{12}$$

Solving for C with the boundary conditions $C = 0$ at $t = 0$ gives

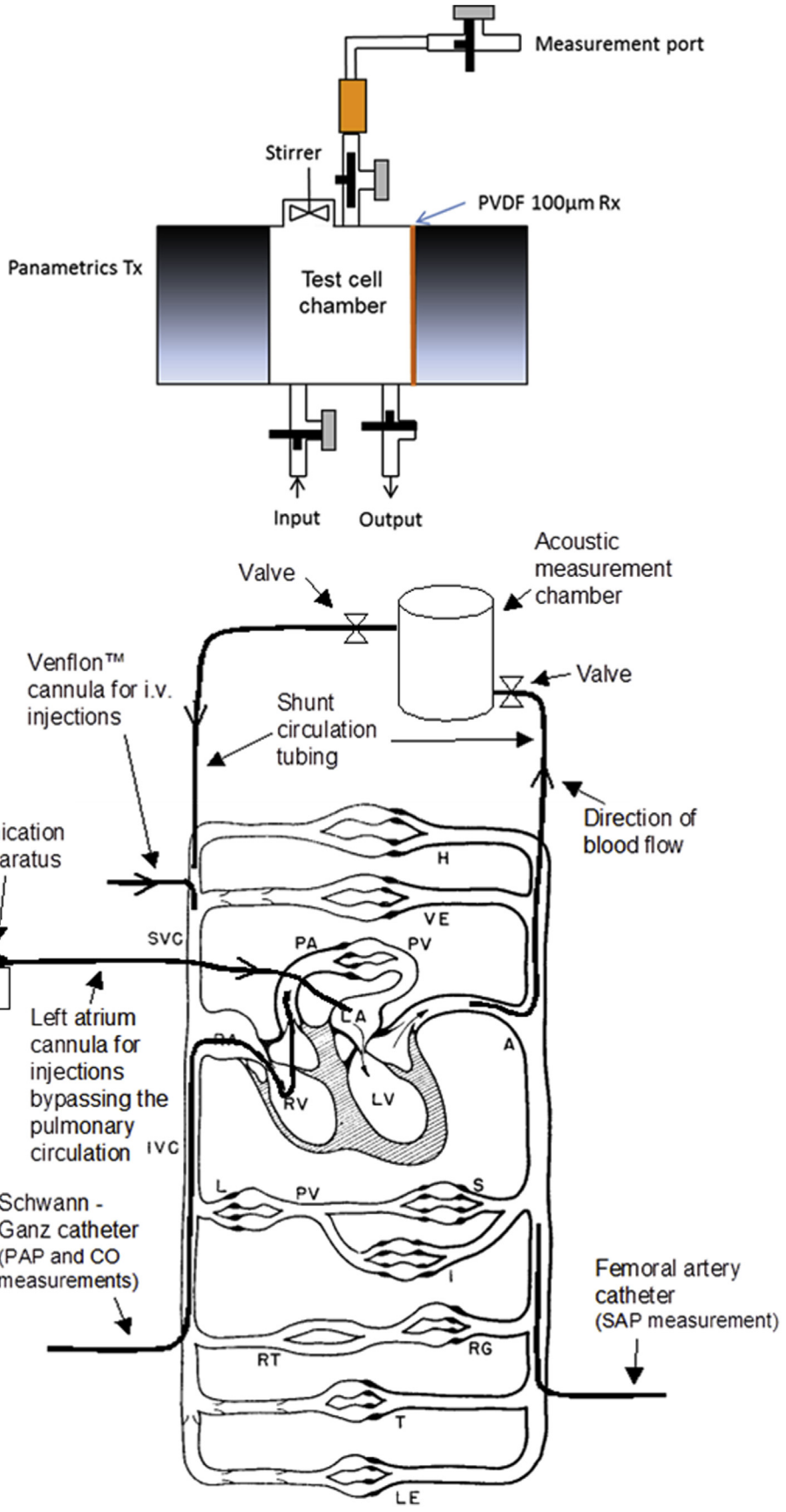
Measurement port
Stirrer
PVDF 100µm Rx
Panametrics Tx
Test cell chamber
Input
Output
Valve
Acoustic measurement chamber
Valve
Venflon™ cannula for i.v. injections
Shunt circulation tubing
Direction of blood flow
Sonication apparatus
H
VE
SVC
PA
PV
LA
A
RA
RV
LV
IVC
Left atrium cannula for injections bypassing the pulmonary circulation
L
PV
S
Schwann - Ganz catheter (PAP and CO measurements)
I
Femoral artery catheter (SAP measurement)
RT
RG
T
LE

$$C = -\frac{c_i e^{-t\alpha_1-\alpha_2 t_t}\left(e^{t\left(-\frac{\dot{Q}}{V_0}+\alpha_1-\alpha_2\right)}-1\right)\dot{Q}}{\dot{Q}+V_0(\alpha_2-\alpha_1)} \quad (13)$$

which gives the cell concentration as a function of time. The maximum concentration c_{max} at time t_{max} is given by

$$c_{max} = \frac{c_i e^{-\alpha_2 t_t} - \frac{V_0\alpha_1 \ln\left(\frac{\dot{Q}+V_0\alpha_2}{V_0\alpha_1}\right)}{\dot{Q}+V_0(\alpha_2-\alpha_1)}\dot{Q}}{\dot{Q}+V_0\alpha_2}, t_{max} = \frac{V_0 \ln\left(\frac{\dot{Q}+V_0\alpha_2}{V_0\alpha_1}\right)}{\dot{Q}+V_0(\alpha_2-\alpha_1)} \quad (14)$$

Setting $\alpha_1 = 0$ gives us the response to a step function,

$$c_{step} = -\frac{c_i e^{-\alpha_2 t_t}\left(e^{-\frac{\dot{Q}}{V_0}t-\alpha_2 t}-1\right)\dot{Q}}{\dot{Q}+V_0\alpha_2} \quad (15)$$

and taking the derivative of c_{step}, $\frac{dc_{step}}{dt}$, gives the impulse response

$$c_{impulse} = \frac{e^{-\frac{\dot{Q}}{V_0}t-(t+t_t)\alpha_2}\dot{Q}}{V_0} \quad (16)$$

V_0 is fixed by the cell dimensions and is 48.5 mL. The length of tubing to the inlet port is 66 cm. The tubing internal diameter is 0.070 in. (~1.78 mm).

Taking the (one-sided) Laplace transform of the impulse response gives

$$\int_0^\infty \frac{e^{-\frac{\dot{Q}}{V_0}t-(t+t_t)\alpha_2}\dot{Q}}{V_0} = \frac{\dot{Q}}{V_0}e^{-t_t\alpha_2}\frac{1}{\left(s+\frac{\dot{Q}}{V_0}+\alpha_2\right)} \quad (17)$$

as

$$\mathrm{Re}\left[\frac{\dot{Q}}{V_0}+\alpha_2\right] > 0 \quad (18)$$

Thus we have a pole located at $s_p = -\left(\frac{\dot{Q}}{V_0}+\alpha_2\right)$, in the s plane. To estimate the concentration entering the cell, c_i (t), we filter the measured cell concentration with a single zero filter located at s_p, with a gain of $\frac{\dot{Q}}{V_0}e^{-t_t\alpha_2}$. To determine the total volume of bubbles liberated, v_{btot}, c_i (t) is multiplied by the cardiac output

$$v_{btot} = \int_0^\infty c_i(t)dt \times \text{cardiac output} \quad (19)$$

Calculation of activation yield

The concentration and size distribution data of the microdroplet emulsion measured with the Coulter Multisizer III is used in the simulation. Activated bubble volume–time curves, v_n (t), were calculated according to the model in the Appendix, using an initial microdroplet diameter corresponding to the mean diameter in each of the n_c Coulter measurement channels. The volume–time curves are then weighted by the number of particles measured in each channel, c_n, and summed to produce a volume–time curve for the bubble population:

$$V_b(t) = \sum_1^{n_c} v_n(t) \cdot c_n \quad (20)$$

The maximum value of V_b (t), v_{bmax}, provides a theoretical peak volume fraction for 100% simultaneous activation of the ACT clusters. The ratio of the measured value from the *in vitro* cell or v_{btot} from the *ex vivo* cell, divided by the theoretical value from eqn (20), provides an estimate of the fraction of clusters activated.

Animal model

Ethical approval was provided by the Norwegian Animal Research Authority (NARA). Three male mixed-breed sibling dogs (Labrador, Harrier) aged 18 mo were used in the study, with weights of (D1) 18 kg, (D2) 17.7 kg and (D3) 17 kg. The dogs were delivered on the morning of the day of the experiment and were anaesthetized immediately without any need for housing.

Anesthesia was induced and maintained with pentobarbital and fentanyl. The animals were ventilated with room air via an orally inserted endotracheal tube and volume-controlled mechanical room air ventilator (New England Model 101 Large Animal Ventilator). The body temperature was kept constant at 38°C with a Harvard homeothermic feedback control unit (rectal temperature sensor controlling an electrical heating blanket). A Swan-Ganz catheter for pressure measurements and monitoring of cardiac output (Baxter Vigilance Continuous Cardiac Output monitor) was inserted into the pulmonary artery via the femoral vein and a groin incision. A systemic arterial pressure transducer catheter was inserted into the femoral artery via the same incision. A 1.4-mm Venflon cannula was inserted in the right cephalic vein proximal to the elbow joint, for injection of test substances.

Fig. 2. Schematic of extracorporeal flow circuit (top) and connections to the animal's circulatory system (bottom). Also depicted are other instrument placements used in the experiment. H = head; VE = upper extremity; PA = pulmonary artery; PV = pulmonary vein; RA = right atrium; LA = left atrium; A = aorta; RV = right ventricle; LV = left ventricle; SVC = superior vena cava; IVC = inferior vena cava; S = sinuses and spleen; I = intestines; L = liver; PV = portal vein; RG = glomerulus in the kidney; RT = renal tubules; T = trunk; LE = lower extremities.

A midline sternotomy was performed, and positive end-expiratory pressure was applied to the respirator outlet when entering the pleural spaces. The anterior pericardium was removed, and the heart was suspended by suturing the rim of the remaining pericardium to the wound edges. The auricular appendix of the left atrium was cannulated for injections of activated ACT drug product, bypassing the pulmonary circulation.

Measurements of bubble size and number in arterial blood were made with the acoustical *ex vivo* extracorporeal measurement chamber described above connected to the circulation of the animal by catheters in the aortic root and the jugular vein. Clotting was prevented by injecting heparin (1000 IU/kg) before connecting and opening the shunt circulation. Blood circulated through the instrument as a consequence of the natural arteriovenous pressure gradient, and the flow rate was on the order of 1.5 mL/s (the actual rate was determined by arterial pressure, blood viscosity and tubing dimensions). This flow corresponds to about 5%–8% of the volume of blood pumped by the heart. Flow rate used in the yield calculations was measured by timed collection of blood from the venous return tubing close to the animal.

An ATL HDI-5000 scanner with a P3-2 transducer was used with an MI scanner setting of 1.0, fundamental B-mode imaging, maximal frame rate (typically 21–40 frames/s), single focal depth set at two-thirds of the left ventricle depth. A short-axis mid-papillary view was used. The depth of the image was adjusted to just cover the distal myocardium. A 30-mm low-attenuation silicone rubber spacer was used between the transducer and the anterior epicardium. Water-based ultrasound coupling gel was used for all acoustical interfaces.

Seven drug product injections were performed per animal, as detailed in Table 1. In addition to measurement in the *ex vivo* system, measurement was also performed in the *in vitro* bubble sizing system in parallel. All sonometry measurements were initiated 10 s before injection. Digital images were recorded and stored in the scanner prior to each injection and 90 s post-injection. In-line activation was used for injections 4 and 5, where ultrasound activation was applied to the catheter line during the injection procedure. The same catheter with in-line activation was also measured in the *in vitro* system. The rate of shrinkage of activated ACT bubbles was studied after intravenous injection and activation by imaging ultrasound. The value of the rate of shrinkage at arterial pressure is required for the yield calculation (the parameter α_2). The flow through the extracorporeal shunt was stopped at peak bolus concentration, about 30 s after injection of the substance. The shunt circulation was stopped either by closing a valve in the arterial line of the shunt or by closing a valve in the venous line. This gave a hydrostatic pressure in the measurement chamber that is either the mean arterial pressure or the venous pressure. Because the measurement chamber was located approximately 25 cm below the level of the animal's heart, the pressure in the chamber became consistently 2.7 kPa higher than the physiologic pressures. The half-time of bubble shrinkage was read directly from the gas volume recording as the time from peak (time point of stopping shunt flow) until the volume was reduced to 50% of the peak value. The pressures were measured from catheter/transducer measurements of arterial pressure, assuming a venous (jugular vein) pressure of zero.

Dosing

The acoustic measurement chamber has a limited range of doses that can be measured, and the dose selected was chosen to span this range. Three doses were administered, 0.63, 1.25 and 2.5 μL drug product/kg body wt, termed half, standard and double, respectively, in Table 1. At least 15 min was given between injections. Injections were performed with an 18G needle through a rubber membrane port on a forelimb Venflon intravenous cannula. On some occasions, injections were performed into the left atrium of the heart via a short polyethylene catheter, either with or without prior activation of the drug product by ultrasound *ex vivo* (in-line activation). Left atrium injections were slow (20 s) to simulate the temporal dispersion of the bolus during normal lung passage. Because of the need for diluting the injected sample for the *ex vivo* ultrasound exposure to penetrate into the fluid, the atrial injections were further diluted with isotonic saline to a total volume of 20 mL.

Table 1. Study design injection list

Task (in sequence)	Injection no.	Dose
Intravenous injection at *in vivo* dose	1	Standard
Catheter administration into the left atrium of *in vivo* dose with imaging activation	2	Standard
Catheter administration into the left atrium with inline acoustic cluster technology activation	3	Standard
Intravenous administration with imaging activation; close venous end of shunt when measurement cell dose is adequate	4	Standard
Intravenous administration with imaging activation; close arterial end of shunt when measurement cell dose is adequate	5	Standard
Intravenous administration with imaging activation	6 and 7	Half and double standard

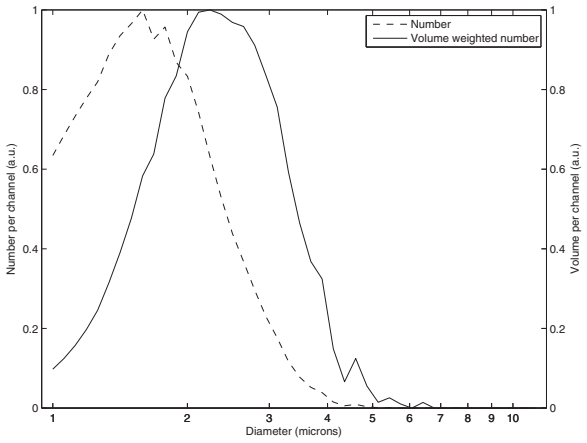

Fig. 3. Normalized Coulter data for emulsion number (*dashed line*) and volume (*solid line*) size distributions.

RESULTS

Simulation results

Coulter sizing of the emulsion droplets is illustrated in Figure 3. The volume-weighted median diameter of the emulsion droplet distribution is 2.8 μm. The simulated radius–time curve for an activated bubble from an initial droplet diameter of 2.8 μm is illustrated in Figure 4, for a bubble in Isoton II at 37°C and 85% air saturation (*in vitro* sonometry cell conditions). The activated bubble reaches a maximum diameter after 12 s of 22.4 μm and has a lifetime of 2 min 55 s. The partial pressure of PFMCP at 37°C is 69 kPa, and bubbles may re-condense at partial pressures above this. However, this occurs when the diameter of the bubble is $<$4 μm and the bubble will be free flowing in the microvasculature. For comparison, a 3.6-μm activated droplet reaches a maximum diameter after 20 s of 29 μm and has a lifetime of approximately 5 min.

Figure 5 is the simulated volume–time curve assuming complete activation of all microdroplets and one microdroplet per cluster (eqn [20]). Illustrated are bubble populations in Isoton II at 37°C and 85% air saturation (*in vitro* sonometry cell conditions) and in blood at 37°C with 98-kPa blood gas saturation and 13.3 kPa blood pressure and 2.7 kPa excess pressure because of the cell being placed 25 cm below the heart (*ex vivo* extracorporeal flow cell conditions). The ratios of the peak gas volumes in the measurement cells to the administered oil volume are 429 and 409 for the *in vitro* and *ex vivo* cell conditions, respectively.

Numerical inversion performance estimates

The bias of the recovered estimate of the volume-weighted full width half-maximum of the bubble population is $<$4%, and the 95% confidence interval is $<$5% of the input simulation values. The bias of the volume-weighted median diameter is less than μm, and the 95%

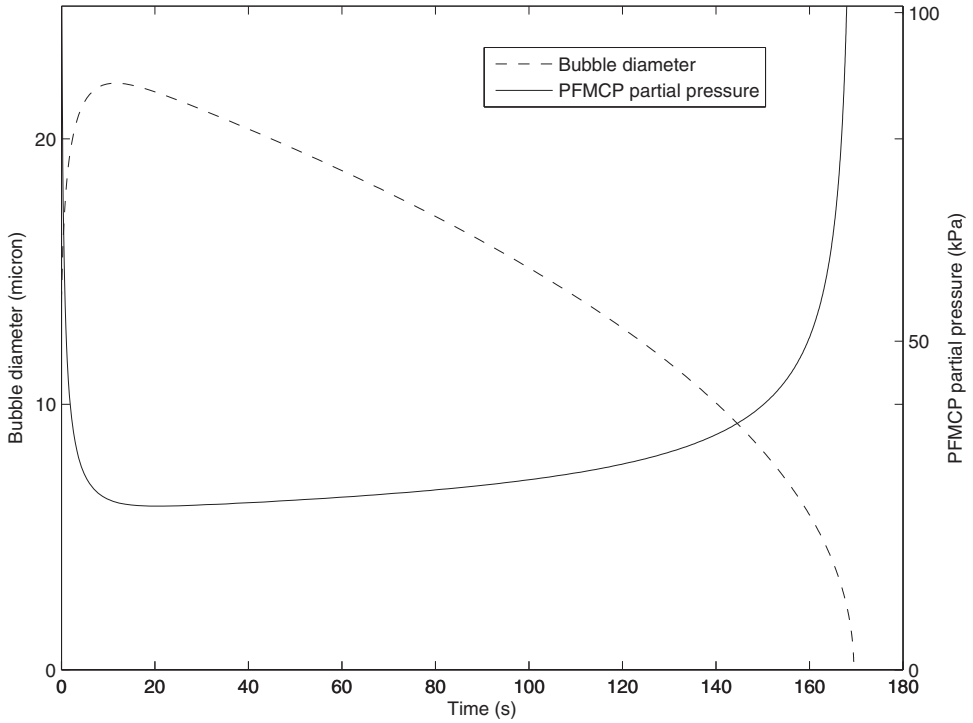

Fig. 4. Simulated radius–time curve for the ACT bubble diameter (*dashed line*) and partial PFMCP inside the bubble (*solid line*), for a 2.8-μm oil droplet in Isoton II at 37°C and 85% gas saturation. The vapor pressure of PFMCP at 37°C is 69 kPa. ACT = activated acoustic cluster technology; PFMCP = pressure of perfluoromethylcyclopentane.

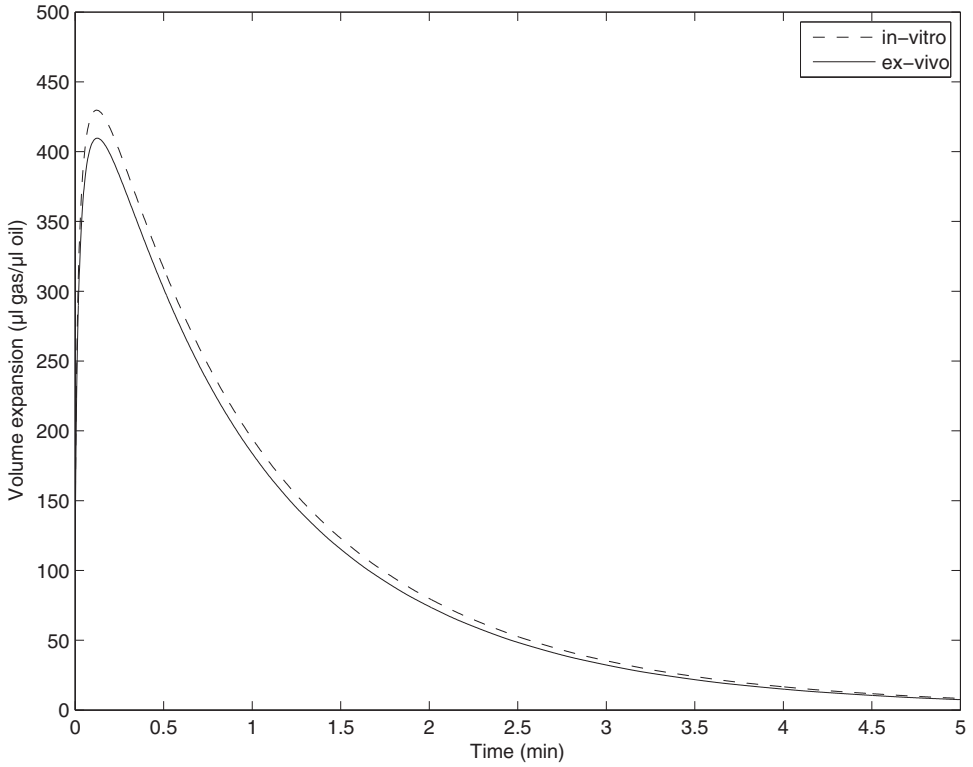

Fig. 5. Simulated volume expansion (μL gas/μL oil) time curves for ACT bubbles from the Coulter distribution illustrated in Figure 3. *Dashed* and *solid lines* represent *in vitro* and *ex vivo* sonometry cell conditions, respectively. ACT = activated acoustic cluster technology.

confidence interval is <1 μm of the input simulation values. For the recovered total bubble volume, there is an approximate -3% bias, and the 95% confidence interval is $<7\%$.

Measurement in vitro

To determine the precision of the sonometry system, six measurements were performed. Two samples from each of three vials were analyzed. The ratio of the peak volume of gas in the measurement chamber to the oil volume administered (μL/μL) had a mean of 389 with a relative standard deviation of 3.5%. Dividing the mean of 389 by the simulated peak gas-to-emulsion volume ratio of 429 for *in vitro* cell conditions gives an estimate of the yield of activation (% volume of oil vaporized) of 91%.

Changing the *in vitro* cell from Isoton II at 37°C and 85% gas saturation to 5% HSA at 37°C and 85% gas saturation produced a reduction in peak gas volume of 51%, reducing the yield of activation to 45%. Parallel-flow particle microscopy analysis of the cluster size distribution was performed under the same dilution medium conditions (Isoton II and HSA). Table 2 indicates that there is a preferential breakup and loss of larger clusters in HSA compared with Isoton II.

Influence of scanner MI on activation in vitro

In vitro activation was quantified for the complete range of scanner outputs (on screen scanner MIs ranging from 0 to 1.0). No activation was measured with the three output settings which displayed an MI of 0.0. There were eight output settings with a displayed MI of 0.1. At the lowest output setting in this range, there was a small amount of activation ($\sim$10% of the peak volume fraction measured with maximal scanner output). At the highest output setting with an onscreen MI of 0.1, activation reached $>90\%$ of the peak volume fraction measured with maximum scanner output. At the first setting with

Table 2. Cluster concentration in acoustic cluster technology test item in various size classes as determined by flow particle image analysis microscopy, measured in 5% human serum albumin and Isoton II

	mill/mL			
Dilution medium	<5 μm	5–10 μm	10–20 μm	20–40 μm
Human serum albumin	154 ± 23	1.6 ± 0.1	nd	nd
Isoton II	128 ± 15	27.5 ± 2	5.4 ± 1.1	0.3 ± 0.2

nd = not detectable.

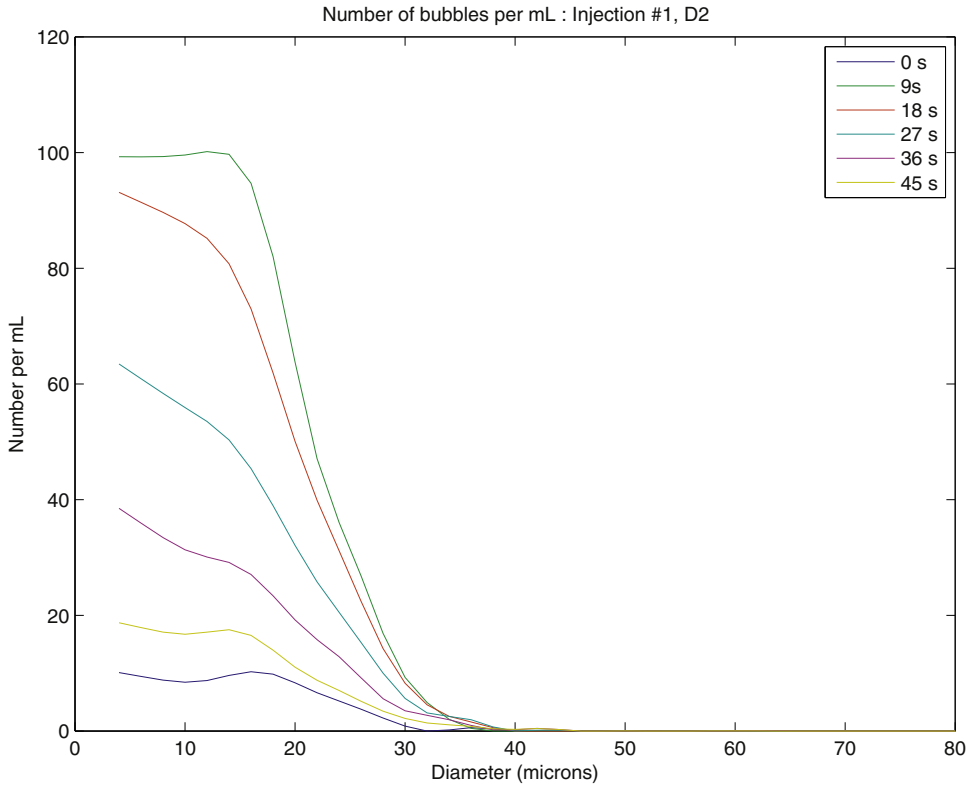

Fig. 6. Three-dimensional bar graph of the calculated number of bubbles in the extracorporeal flow circuit for injection 1 in animal D2.

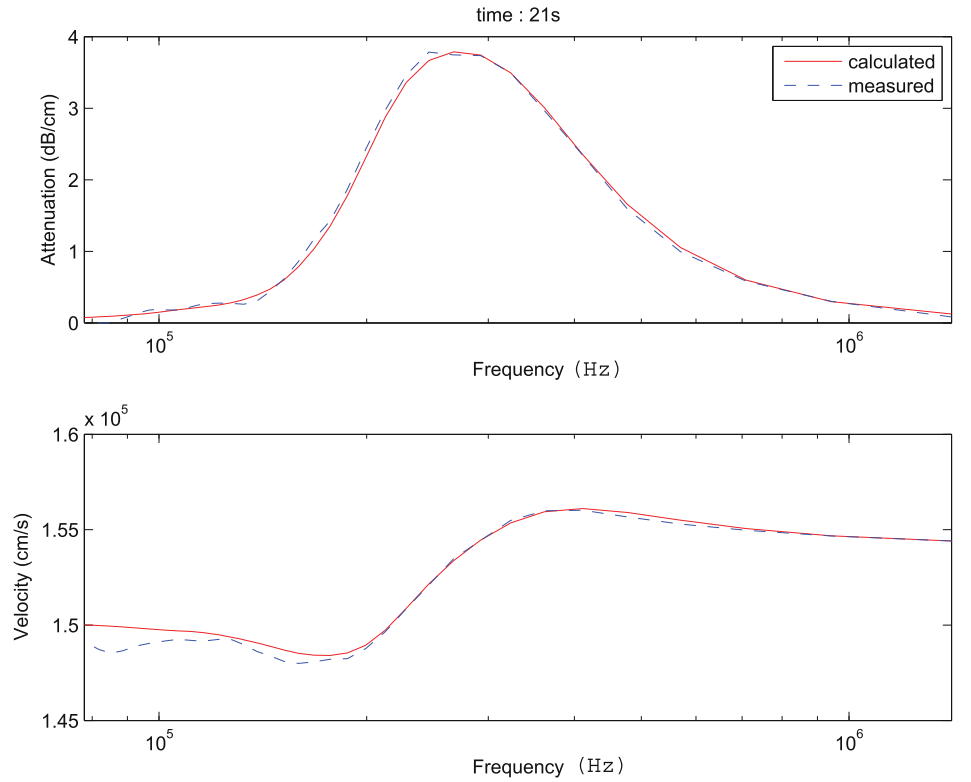

Fig. 7. Measured data and modeled data for (top) acoustic attenuation used in the inversion procedure and (bottom) velocity dispersion used for calculating the quality metric Q_m. The data illustrated are from the maximum volume fraction time point in injection 1 in animal D2 (see Fig. 6).

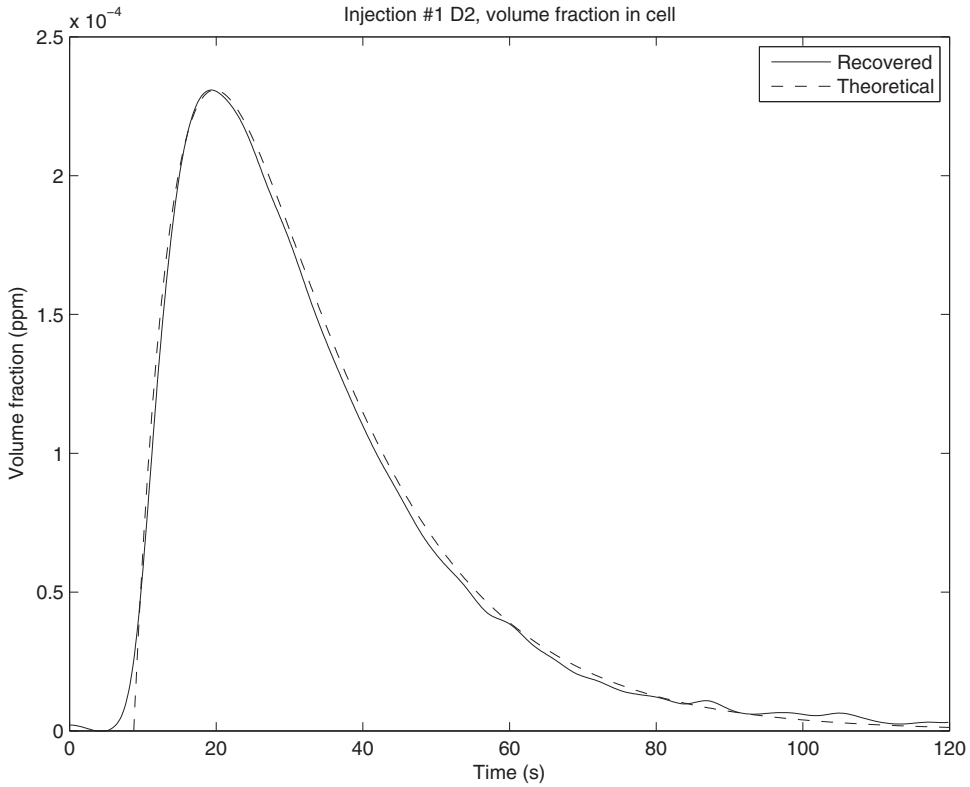

Fig. 8. Volume–time curve for the activated acoustic cluster technology bubble population in the extracorporeal flow circuit from injection 1 in animal D2. The *broken line* represents the theoretical relative volume–time curve from eqn (13).

a displayed output of 0.2, a 100% peak volume fraction was measured, which remained constant for all subsequent output settings up to a displayed MI of 1.0.

The MI is defined as $\mathrm{MI} = \frac{p_{r.3}(z_{sp})}{\sqrt{f_c}}$, where $p_{r.3}(z_{sp})$, is the peak rarefractional pressure derated by 0.3 dB/cm/MHz, to the point on the beam axis where pulse intensity is maximum. f_c is the center frequency of the transmitted pulse. The index is made unitless by multiplying by $[(1\ \mathrm{MHz})^{0.5}/(1\ \mathrm{MPa})]$. Compensation for derating if attenuation is considered negligible in the *in vitro* measurement cell provides an MI of 2.4 experienced by the ACT clusters with the imaging system and scanning mode used here, for maximal activation.

Measurements in extracorporeal flow circuit

A typical example after intravenous injection of the recovered number of bubbles in the extracorporeal flow circuit as a function of time is illustrated in Figure 6 (D2 injection 1). Selected time points have been chosen for clarity of display from measurements performed once every 3 s. The measured attenuation and velocity dispersion and modeled values from the inversion procedure used to calculate bubble number density at the time of peak volume concentration in the cell are illustrated in Figure 7. The value of the parameter Q_m, which indicates the quality of the inversion for this measurement, is 0.96.

The recovered bubble population volume concentration in the extracorporeal flow circuit for injection 1 at the time of peak volume fraction in animal D2 is illustrated in Figure 8, along with the predicted values from eqn (13). Only the first 2 min of measurement data is shown for clarity of display. The inversion quality metric, Q_m, was >0.95, indicating reliable inversion data, when the volume concentration was above 0.5 ppm. The recovered arterial concentration after correction for cardiac output, flow through cell, transit time to cell and bubble population lifetime is shown in Figure 9. The recovered volume-weighted activated bubble population size distribution for injection 1, at the time of peak volume concentration in D2, is illustrated in Figure 10 along with the predicted size distribution from the model (at the time of peak volume concentration). There are no bubbles >44 μm in diameter.

The volume-weighted bubble diameters after intravenous injection (injections 1, 6 and 7) measured under arterial conditions are given in Table 3. The mean value of these observations is 21.4 μm. The values after left atrium injection are given in Table 3

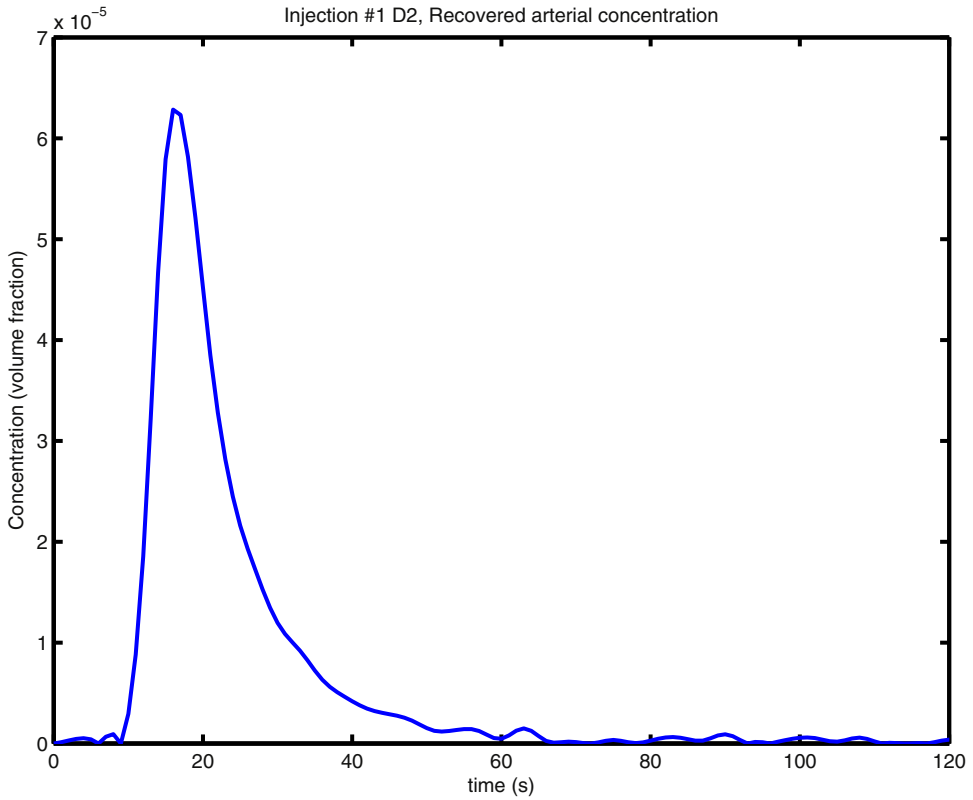

Fig. 9. A blood concentration recovered from the data in Figure 8.

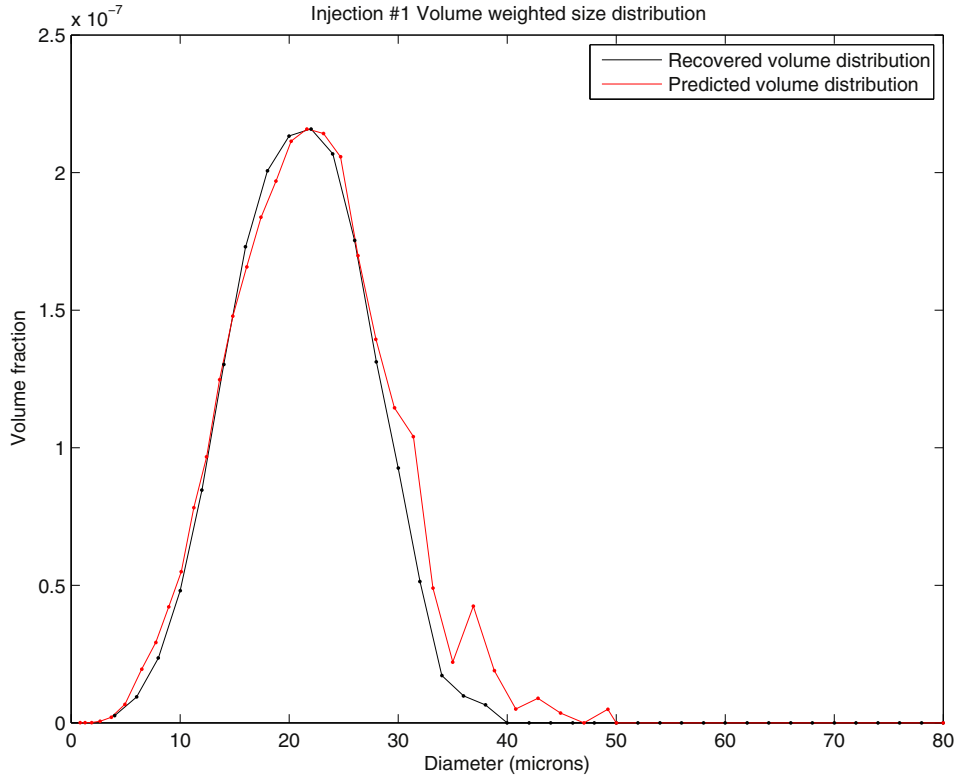

Fig. 10. Recovered bubble distribution from injection 1 in D2 is represented by the *black line*, with bin locations indicated by the *dots*. The simulated distribution for conditions in the extracorporeal cell predicted from the emulsion Coulter data in Figure 1 is represented by the *red line* (amplitude normalized to the peak in the recovered distribution).

Table 3. Volume-weighted median diameters for injections 1, 2, 6 and 7 in the three dogs*

	Diameter (μm)		
Injection no.	Dog 1	Dog 2	Dog 3
1	19.7	22.2	20.5
2	22.0	25.3	23.4
6	21.7	22.3	21.8
7	21.3	21.3	21.6

* Injection 2 is the left atrium injection. Injections 1, 6 and 7 are for intravenous administration.

(injection 2). The mean of these observations is 23.6 μm. Note that the bubbles are slightly larger than after intravenous injection, but not significantly so (paired t-test, $p = 0.16$).

Measurements for the rate of shrinkage of the ACT bubbles at arterial and venous pressures for the three animals are listed in Table 4. The mean values at arterial and venous pressures are 20 and 36 s, respectively. There is faster decay at arterial pressure (paired t-test, $p = 0.002$) caused by the elevated partial pressure of all gases inside the bubbles, giving larger gradients for outward diffusion. The measured 20-s value was used for the value of α_2 in eqn (19) for the *ex vivo* yield calculation.

Yield of activation. Table 5 lists the calculated yield of activation after intravenous injection. Note that animal D2 has higher values than the other two animals. The mean (standard error of the mean [SEM]) of all measurements is 24.4% (2.5%). The yield of activation after left atrium injections is given in Table 5 (injection 2). The mean (SEM) of all measurements is 69.7% (6.2%). Note that the yield is higher after left atrium injection than after intravenous injection (two-sample t-test, $p = 0.019$).

In vitro *to* ex vivo *yield comparison.* To verify the operation of the extracorporeal shunt measurements and the yield calculation, control analysis was performed using *ex vivo* and *in vitro* bubble sizing. The in-line catheter activation delivered the same dose of activated bubbles directly into the left atrium (measured in the extracorporeal chamber) and into the *in vitro* chamber. Ultrasound imaging activation in the left ventricle was suspended during this *in vivo* injection. The ratio of calculated yield measured *ex vivo* to the yield *measured in vitro* was 0.81, 1.05 and 0.95 for D1, D2 and D3, respectively (mean = 0.94), showing consistency between the *in vitro* and *ex vivo* yield calculations.

Table 5. Yield of activation*

Injection no.	Dog 1	Dog 2	Dog 3
2	72.2%	79.0%	58.0%
1	16.3%	27.1%	16.7%
6	25.2%	35.3%	20.1%
7	22.7%	36.6%	19.3%
Mean	21.4%	33.0%	18.7%

* Injection 2 is the left atrium injection. The mean is the mean of intravenous injections 1, 6 and 7.

Bubble numbers for intravenous injections. The inversion procedure recovers bubble numbers with diameters in 2-μm bins from 4 to 80 μm. The bubble numbers produced were classified into two groups: bubbles with diameters from 10 to 25 μm and bubbles with diameters >25 μm. The numbers produced for all intravenous injections are listed in Table 6 and are dose and weight corrected to a dose of 10 μL drug product/kg body wt. Ninety-one percent (SEM = 0.5%) of the bubbles are in the size group 10–25 μm.

B-Mode imaging contrast enhancement and number of activated bubbles. B-Mode contrast enhancement in the myocardium was calculated by linearizing the digital images acquired with the ATL scanner before and 90 s after injection (see Fig. 11 for example images). The echo enhancement relative to myocardium (linear backscatter intensity divided by linear backscatter intensity with no agent present) tissue background is plotted as a function of measured total bubble numbers per kilogram body weight in Figure 12. A least-sum-of-squares regression line with a forced zero intercept is shown with a slope of 281 mg/bubble. This indicates that a dose corresponding to one activated ACT bubble per 281 mg myocardial tissue (3560 bubbles/kg) will generate an echo enhancement equal to the baseline echo.

The slope of the regression line fitted to the measured bubble number from intravenous injection versus dose of drug product is 56×10^6 bubbles/mL drug product. This allows calculation of the total number of activated bubbles (N) at a typical imaging dose of 10 μL drug product/kg body wt, in an 18-kg animal:

Table 4. Volume half-time at arterial and venous pressures

	Dog 1		Dog 2		Dog 3	
	Pressure in chamber	Half-time	Pressure in chamber	Half-time	Pressure in chamber	Half-time
Arterial	87 mm Hg	21 s	87 mm Hg	18 s	88 mm Hg	21 s
Venous	20 mm Hg	38 s	20 mm Hg	33 s	20 mm Hg	36 s

Table 6. Estimated total numbers of bubbles in arterial blood after intravenous injection and ultrasound imaging activation*

	Dog 1		Dog 2		Dog 3	
Injection no.	10–25 μm	>25 μm	10–25 μm	>25 μm	10–25 μm	>25 μm
1	0.422×10^6	0.034×10^6	0.468×10^6	0.055×10^6	0.357×10^6	0.026×10^6
6	0.373×10^6	0.039×10^6	0.618×10^6	0.073×10^6	0.333×10^6	0.035×10^6
7	0.389×10^6	0.040×10^6	0.727×10^6	0.073×10^6	0.348×10^6	0.034×10^6
Mean	0.395×10^6	0.038×10^6	0.605×10^6	0.067×10^6	0.346×10^6	0.032×10^6

* The numbers have been adjusted to correct for the different dose levels used (to 10 μL drug product/kg body wt).

$$N = \frac{56 \cdot 10^6}{\text{ml}} \cdot 10 \frac{\mu\text{L}}{\text{kg}} \cdot 18\text{kg} \approx 1.0 \cdot 10^7 \qquad (21)$$

Cardiac output (CO) was measured to be 1900 mL/min. Assuming a normal perfusion in resting myocardium (Q_c) of 70 mL/min per 100 mL tissue, the number concentration of deposited bubbles in myocardial tissue (C_N) after injection of 10 μL/kg ACT is

$$C_N = N \cdot \frac{Q\text{c}}{\text{CO}} = 1.0 \cdot 10^7 \cdot \frac{70 \cdot \frac{\text{mL}}{\text{min} \cdot 100\text{mL}}}{1900 \frac{\text{mL}}{\text{min}}} \approx \frac{3700}{\text{mL}} \qquad (22)$$

or about 4 bubbles/mm^3 (at the 10 μL/kg drug product dose). Similar calculations might be performed for all other tissues receiving an arterial blood supply if their perfusion is known.

DISCUSSION AND CONCLUSIONS

Figure 6 illustrates the inversion data for the bubble population number distribution with measurements performed once every 3 s. There is a good correlation across measurement time points. The inversion model-versus-measurement plots in Figure 7 indicate a good fit to the model, as quantified by the inversion quality metric. The analytical precision observed in the *in vitro* measurements indicates a robust methodology, strongly corroborated by the consistency between results obtained from *in vivo* activation and measurements in the extracorporeal chamber.

The vast majority of ACT bubbles generated *in vivo* are <40 μm in diameter. Table 3 indicates that the volume weighted median diameter lies between 20 and 22 μm, from intravenous administration. Table 6 indicates that 91% of the ACT bubbles generated are <25 μm in diameter. This implies that the ACT bubbles are likely to lodge at the capillary level. In Figure 8 is a typical measured bubble population distribution (at peak volume in the cell), which indicates good correspondence between the experimental data and model predictions from the emulsion Coulter characterization data. Figure 10 is the volume–time curve from a typical *ex vivo* measurement from intravenous injection. The simple model used to calculate yield indicates a good fit to the measured data.

The activation yield in the *in vitro* measurement chamber is 91% and drops to 45% when the fluid in the chamber is changed from Isoton II to HSA. On the basis of the microscopy data in Table 2, this reduction is apparently due to a disintegration of clusters. HSA more

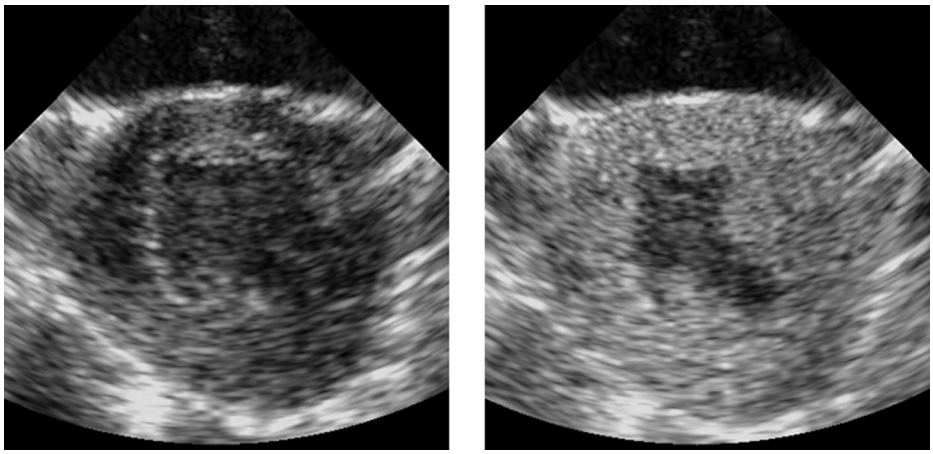

Fig. 11. B-Mode images of dog myocardium (left) before and (right) 60 s after acoustic cluster technology left atrium injection at a dose of 2.5 μL drug product/kg body wt. There is a 17-dB increase in myocardial backscatter in fundamental B-mode.

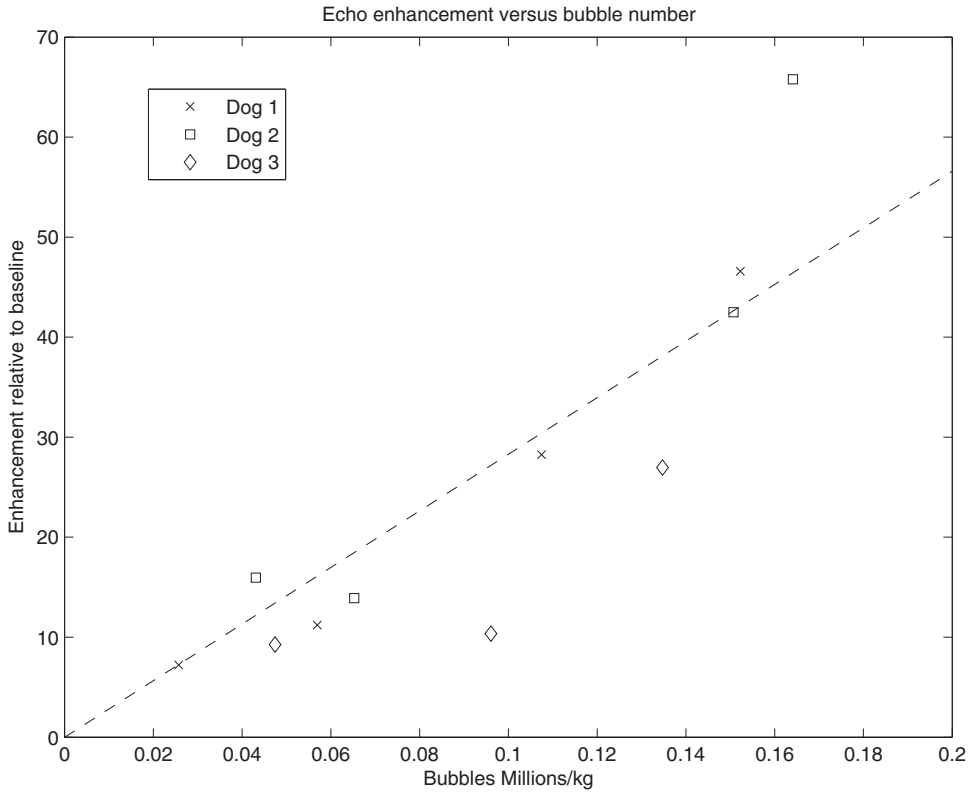

Fig. 12. Myocardial echo contrast as a function of bubble number. Crosses = animal D1, squares = animal D2, diamonds = animal D3. Data for both intravenous and intra-atrial injections are included. The *dashed line* is the regression line with a slope of 281 mg.

closely mimics the *in vivo* whole-blood environment. Similarly, on intra-atrial administration of ACT (bypassing the pulmonary circulation), a 69% yield of activation is measured, which drops to 24% (a loss of 65% by gas volume) on intravenous administration. Breakup of larger clusters in whole blood may account for the majority of this reduction on intravenous administration, as indicated by the *in vitro* measurements in Isoton II and HSA. Other mechanisms may include "trapping" of larger clusters or a small fraction of activated bubbles in the lung capillaries. The ultrasound threshold of activation for ACT clusters is low (MI $>$0.1), and it is feasible that there is some exposure of the right ventricle to ultrasound capable of activating a portion of the compound in the pulmonary circulation with subsequent trapping in the lungs.

The acoustic inversion methodology has been validated in the literature (Wu and Chahine 2010), by comparison with optical photography (10 to 3000 μm range). Similar validation measurements have been performed with optical microscopy for the sonometry system (Sontum et al. 2015a). *In silico* simulation around the operating point of the *ex vivo* extracorporeal cell indicates a robust inversion procedure, assuming the bubble model is correct.

The model of bubble growth and dissolution described in this article has several limitations. It does not contain the gas contribution from the microbubble in the cluster. However, as microbubbles and oil microdroplets are of similar volume, this error term is on the order of a few percent of the final bubble volume and can be neglected. The parameters used for diffusion and Ostwald coefficients are not for whole blood. The values for common (air) gas coefficients in blood and tissue are scarce and have been reviewed (Langø et al. 1996). Solubility coefficients for water may be used as a good approximation, apart from fatty tissues. The PFMCP oil used is a perfluorinated hydrocarbon. The carbon–fluorine bond is powerful (120 kcal/mol). Because of the very powerful bonds, PFCs cannot bind to any protein or enzyme (Spiess 2009) although they are more soluble in lipid membranes, and thus, it is assumed that there is no "sink" due to protein binding that may significantly alter solubility. However, the PFMCP solubility value used in the simulation is calculated and only an order of magnitude estimate. The main shortcoming of the bubble growth and dissolution model is that it is for a stationary bubble in a fluid and does not incorporate a convective term. This may be more appropriate for bubbles "trapped" in the microvasculature, but bubbles not trapped

will experience a convective term, that is, the *in vitro* and *ex vivo* measurement cells which incorporate stirring. Thus, bubble populations in the measurement chambers are expected to have shorter lifetimes than those deposited in tissue. A mathematical model has been reported (Branger and Eckmann 1999) for examining the effect of the cylindrical nature of a bubble trapped in the microvasculature on its lifetime. The model gives longer bubble lifetimes (≤50%) than for spherical bubbles, which has also been observed *in vivo* (Branger and Eckmann 1999; Branger et al. 2001).

With the limitations and shortcomings stated, based on the consistency between the modeled and measured data, the model does seem to predict with reasonable accuracy the behavior of the ACT system, both *in vitro* and *in vivo*.

As the ACT bubbles are much larger (20–30 μm diameter) than conventional commercially available contrast agents (1–6 μm), they are able to produce significant backscatter in fundamental imaging mode at low dose (see Figs. 11 and 12). The number of activated bubbles at a dose of 10 μL drug product/kg body wt has been estimated to be 10 million. This number gives a myocardial echo enhancement of approximately 30 dB in fundamental imaging mode.

The measurements of bubble number generated after injection of a dose are based on indirect measurements in the *ex vivo* chamber connected to the animal's circulation system. Only a small fraction of the injected substance will be diverted into the analysis chamber, and determination of total bubble numbers depends on calculations that incorporate variables such as the actual flow through the extracorporeal shunt, the volume inside the chamber and the cardiac output of the animal (as measured by thermodilution). Verification of correct measurements and calculations in all animals was obtained by parallel *in vitro* analysis with in-line sonication activation of the injected samples.

The current study has demonstrated the ability to perform accurate and reproducible measurements of activated ACT bubble numbers and size, both *in vitro* and in arterial blood of dogs. The measured bubble numbers are closely related to imaging efficacy (Fig. 12).

Acknowledgments—The authors thank Roald Skurtveit, Ove M. Moen, Henrik Rasmussen, Anne-Marie Hvoslef and Eva Gustavssen for their technical assistance.

REFERENCES

Ainslie MA, Leighton TG. Review of scattering and extinction cross-sections, damping factors, and resonance frequencies of a spherical gas bubble. J Acoust Soc Am 2011;130:3184–3208.

Apfel R.E., "Activatable infusable dispersions containing drops of a superheated liquid for methods of therapy and diagnosis," U.S. Patent 5 840 276, 1998.

Branger AB, Eckmann DM. Theoretical and experimental intravascular gas embolism absorption dynamics. J Appl Physiol 1999;87:1287–1295.

Branger AB, Lambertsen CJ, Eckmann DM. Cerebral gas embolism absorption during hyperbaric therapy: Theory. J Appl Physiol 2001;90:593–600.

Burkard ME, Van Liew HD. Simulation of exchanges of multiple gases in bubbles in the body. Respir Physiol 1994;95:131–145.

Butler DB, Hills BA. The lung as a filter for microbubbles. J Appl Physiol 1979;47:537–543.

Castle J, Butts M, Healey A, Kent K, Marino M, Feinstein SB. Ultrasound-mediated targeted drug delivery: Recent success and remaining challenges. Am J Physiol Heart Circ Physiol 2013;304:H350–H357.

Chatterjee D, Sarakar K, Jain P, Schreppler NE. On the suitability of broadband attenuation measurement for characterizing contrast microbubbles. Ultrasound Med Biol 2005;31:781–786.

Commander KW, McDonald RJ. Finite element solution of the inverse problem in bubble swarm acoustics. J Acoust Soc Am 1991;89:592–597.

Commander KW, Prosperetti A. Linear pressure waves in bubbly liquids: Comparison between theory and experiment. J Acoust Soc Am 1989;89:732–746.

Doinikov AA, Sheeran PS, Bouakaz A, Dayton PA. Vaporization dynamics of volatile perflurocarbon droplets: A theoretical model and in vitro validation. Med Phys 2014;41:102901.

Domenech RK, Hoffman JI, Noble MI, Saunders KB, Henson JR. Total and regional coronary blood flow measured by radioactive microspheres in conscious and anesthetized dogs. Circ Res 1969;25:581–596.

Duraiswami R. Bubble density measurement using an inverse scattering technique. Cavitation Multiphase Flow 1993;153:67–73.

Eriksen M, Tolleshaug H. Improvements in or relating to contrast agents. World Patent WO 99/53963; 1999.

Foldy LL. The multiple scattering of waves. I. General theory of isotropic scattering by randomly distributed scatterers. Phys Rev B 1945;67:107–119.

Hayduk W, Laudie H. Prediction of diffusion coefficients for nonelectrolytes in dilute aqueous solutions. AIChE J 1974;20:611–615.

Hogg JC. Neutrophil kinetics and lung injury. Physiol Rev 1987;67:1249–1295.

Iyer AK, Khaled G, Fang J, Maeda H. Exploiting the enhanced permeability and retention effect for tumor targeting. Drug Discov Today 2006;11:812–818.

Kabalnov A, Klein D, Pelura T, Schutt E, Weers J. Dissolution of multicomponent microbubbles in the bloodstream: 1. Theory. Ultrasound Med Biol 1998;24:739–749.

Kausik S, Katiyar A, Jain P. Growth and dissolution of an encapsulated contrast microbubble: Effects of encapsulation permeability. Ultrasound Med Biol 2009;35:1385–1396.

Kripfgans OD, Fowlkes JB, Miller DL, Eldevik OP, Carson PL. Acoustic droplet vaporization for therapeutic and diagnostic applications. Ultrasound Med Biol 2000;26:1177–1189.

Langø T, Mørland T, Brubakk AO. Diffusion coefficients and solubility coefficients for gases in biological fluids and tissues: A review. Undersea Hyperb Med 1996;23:247–272.

Lawson CL, Hanson RJ. Solving least squares problems. Englewood Cliffs, NJ: Prentice Hall; 1974.

Lin CY, Pitt WG. Acoustic droplet vaporisation in biology and medicine. BioMed Res Int 2013;2013:404361.

Lo AH, Kripfgans OD, Carson PL, Rothman ED, Fowlkes JB. Acoustic droplet vaporization threshold: Effects of pulse duration and contrast agent. IEEE Trans Ultrason Ferroelectr Freq Control 2007;54:933–946.

Østensen J, Eriksen M, Frigstad S, Rongved P. Improvements in or relating to contrast agents. World Patent WO 98/17324; 1998.

Qin S, Caskey CF, Ferrara KW. Ultrasound contrast microbubbles in imaging and therapy: Physical principles and engineering. Ultrasound Med Biol 2009;54:R27–R57.

Rapoport N. Phase-shift, stimuli-responsive perfluorcarbon nanodroplets for drug delivery to cancer. Interdiscip Rev Nanomed Nanobiotechnol 2012;4:492–510.

Rosina J, Kvašňák E, Šuta D, Kolářová H, Málek J, Krajči L. Temperature dependence of blood surface tension. Physiol Res 2007;56: S93–S98.

Sheeran PS, Dayton PA. Phase change contrast agents for imaging and therapy. Curr Pharm Des 2012;18:2152–2165.

Shpak O, Stricker L, Versluis M, Lohse D. The role of gas in ultrasonically driven vapour bubble growth. Phys Med Biol 2013;58: 2523–2535.

Shpak O, Verweij M, Vos HJ, de Jong N, Lohse D, Versluis M. Acoustic droplet vaporization is initiated by superharmonic focusing. Proc Natl Acad Sci U S A 2014;111:1697–1702.

Sontum PC. Physicochemical characteristics of Sonazoid, a new contrast agent for ultrasound imaging. Ultrasound Med Biol 2008; 34:824–833.

Sontum PC, Healey AJ, Kvåle S. Delivery of drugs. Patent application PCT/NO2014/050177. Available at: https://patentscope.wipo.int/search/en/detail.jsf?docId=WO2015047103&redirectedID=true; 2015a. Accessed December 20, 2015.

Sontum PC, Kvåle S, Healey AJ, Skurtveit R, Watanabe R, Matsumura M, Østensen J. Acoustic cluster therapy (ACT): A novel concept for ultrasound mediated, targeted drug delivery. Int J Pharm 2015b;495:1019–1027.

Spiess BD. Perfluorocarbon emulsions as a promising technology: A review of tissue and vascular gas dynamics. J Appl Physiol 2009;106: 1444–1452.

Twerski V. On scattering of waves from random distributions: I. Free space scatterer formalism. J Math Phys 1962;3:700–715.

Vagle S, Farmer D. A comparison of four methods for bubble size and void fraction measurements. IEEE J Oceanic Eng 1998;23:3.

Van Liew HD, Burkard ME. Bubbles in circulating blood: Stabilisation and simulations of cyclic changes of size and content. J Appl Physiol 1995a;79:1379–1385.

Van Liew HD, Burkard ME. Behavior of bubbles of slowly permeating gas used for ultrasonic imaging contrast. Invest Radiol 1995b;30: 315–321.

Waterman PC, Truell R. Multiple scattering of waves. J Math Phys 1961; 2:512–537.

Wong Z, Kripfgans OD, Qamar A, Fowlkes JB, Bull J. Bubble evolution in acoustic droplet vaporization at physiological temperature via ultra-high speed imaging. Soft Matter 2011;7:4009–4011.

Wood AKW, Sehgal CM. A review of low-intensity ultrasound for cancer therapy. Ultrasound Med Biol 2015;4:905–928.

Wu X, Chahine GL. Development of an acoustic instrument for bubble size distribution measurement. J Hydrodynam Ser B 2010;22:330–336.

APPENDIX

Dynamic bubble growth model

For the initial vaporization of the oil droplet, assuming an ideal gas, the volume of gas at a given pressure inside the bubble, p_b, liberated from a volume of oil is given as (ignoring the volume of gas contributed by the Sonazoid bubble)

$$V_g(v_{pf}, p_b) = \frac{v_{pf} \times \rho_{pf} \times N_a \times k_b \times T}{mw_{pf} \times p_b} \tag{A1}$$

Body temperature is assumed to be 310 K. Assuming spherical bubbles and liquid droplets, and zero surface tension, the expression for the bubble diameter as a function of droplet diameter at a given pressure is given by

$$D_b(p_b, D_d) = \sqrt[3]{\frac{\rho_{pf} \times N_a \times k_b \times T}{mw_{pf} \times p_b}} \times D_d \tag{A2}$$

If we include surface tension, the expression for pressure is

$$P_w = p_b - \frac{4\tau}{D_b(p_b, D_d)} \tag{A3}$$

Combining equations we have a cubic for the bubble diameter:

$$P_w D_b^3 + 4\tau D_b^2 - C = 0, C = \frac{v_{pf} \times \rho_{pf} \times N_a \times k_b \times T \times 6}{mw_{pf} \times \pi} \tag{A4}$$

The solution is the real valued root:

$$D_b = -\frac{1}{3(P_w - p_w)} \left(4\tau + \frac{-1 + i\sqrt{3}}{2} c + \frac{2}{-1 + i\sqrt{3}} \frac{\Delta_0}{c} \right) \tag{A5}$$

$$c = \sqrt[3]{\frac{\Delta_1 + \sqrt[2]{\Delta_1^2 - 4\Delta_0^3}}{2}}, \Delta_0 = 16\tau^2, \Delta_1 = 128\tau^3 - 27(P_w - p_w)^2 C \tag{A6}$$

For 3.6- and 2.8-μm PFMCP droplet diameters, vapor droplets diameters are 18.23 and 14.04 μm, respectively (at atmospheric pressure in Isoton II at 37°C).

After vaporization there will be an initial inward diffusion of blood gases and water vapor, causing further bubble expansion, and an outward diffusion of PFMCP. A model for the growth and dissolution process based on Kabalnov et al. (1998) is presented next.

At mechanical equilibrium, we have

$$(C_{pf} + C_A) RT = p_A + p_{pf} = \frac{2\tau}{r} + p_{atm} + p_{blood} \tag{A7}$$

The steady-state diffusional flux is

$$J_{pf} = -\frac{d}{dt} \left[\frac{4\pi}{3} (C_{pf} r^3) \right] = 4\pi r D_{pf} \left[c_{pf}(r) - c_{pf}(\infty) \right] \tag{A8}$$

With the obvious analogous definition for J_A. It is assumed that $c_{pf}(\infty) = 0$; thus, we have

$$-\frac{d}{dt}(C_{pf} r^3) = 3 r D_{pf} L_{pf} C_{pf}, -\frac{d}{dt}(C_A r^3) = 3 r D_A L_A \left(C_A - \frac{p_{air}}{RT} \right) \tag{A9}$$

Here we allow for under saturation of air by incorporation of the term $\frac{p_{air}}{RT}$. We use the following dimensionless parameters and variables:

$$\mu = \frac{2\tau}{p_{atm} r_0}; \vartheta = \frac{p_{blood}}{p_{atm}}; \rho = \frac{r}{r_0}, \delta = \frac{D_A}{D_{pf}}, \chi_A = \frac{C_A RT}{p_{atm}},$$

$$\chi_{pf} = \frac{C_{pf} RT}{p_{atm}}, \Gamma = \frac{D_{pf}}{r_0^2} t \tag{A10}$$

$$F = \chi_{pf} \rho^3, A = \chi_A \rho^3, p_d = \frac{p_{air}}{p_{atm}}$$

One obtains

$$F + A = \mu\rho^2 + (1 + \vartheta)\rho^3, \frac{dF}{d\Gamma} = -\frac{3L_{pf}}{\rho^2} F, \frac{dA}{d\Gamma} = -\frac{3\delta L_A}{\rho^2} (A - p_d \rho^3) \tag{A11}$$

Eliminating variables, we arrive at the expression

$$\frac{d\rho}{d\Gamma} = \frac{-3\delta L_A (A - p_d \rho^3) - 3L_{pf} (\mu\rho^2 + (1 + \vartheta)\rho^3 - A)}{\rho^3 (2\mu + 3(1 + \vartheta)\rho)} \tag{A12}$$

We now have three differential equations with initial conditions

$$F(0) = X_{pf}(\mu + \vartheta + 1), A(0) = (1 - X_{pf})(\mu + \vartheta + 1), \rho(0) = 1 \tag{A13}$$

where X_{pf} is the mole fraction of PFMCP at $t = 0$. This system is in a form that can be solved numerically with an ordinary differential equation solver.

Selection of parameters

The values of the parameters used in the simulations are summarized in Table A1.

Surface tension. The value for surface tension in Isoton II of 0.052 N/m was used. Isoton II contains 0.3% by weight ethylene glycol phenyl ether, which may reduce this value for the bubble surface, so this is an upper limit. The value of v_{bmax} determined from the simulation (eqn [20]) increases by <10% when the surface tension is reduced to 0.035 N/m. The value of the surface tension of blood is taken to be 0.052 N/m (Rosina et al. 2007).

Diffusion coefficients. The diffusion coefficient of PFMCP was estimated using the Hayduk–Laudie equation for the molecular volumes of fluorocarbons (Hayduk and Laudie 1974):

$$D = 13.26 \cdot 10^{-5} \times \eta^{-1.14} \times V_m^{-0.589} = 9.6241 \cdot 10^{-10} \mathrm{m}^2/\mathrm{s} \tag{A14}$$

The dynamic viscosity of water at 37°C was employed, estimated using

$$A \times 10^{\frac{B}{(T-C)}} = 0.69244 \text{ mPa·s; A} = 2.414 \cdot 10^5 \text{ (Pa·s); B} = 247.8 \text{ K;}$$
$$\text{C} = 140 \text{ K} \tag{A15}$$

The diffusion of air in water at 25°C is 2.00 × 10^{-9} m^2/s. An approximate dependence of the diffusion coefficient on temperature in liquids can often be found using the Stokes–Einstein equation, which predicts that

$$\frac{D_{T_1}}{D_{T_2}} = \frac{T_1}{T_2} \times \frac{\mu_{T_2}}{\mu_{T_1}} \tag{A16}$$

where T_1 and T_2 denote temperatures 1 and 2, respectively, D is the diffusion coefficient (cm^2/s). T is the absolute temperature (K) and μ is the dynamic viscosity of the solvent (Pa·s). This gives an estimate of 2.6847 × 10^{-9} m^2/s at 37°C.

Water solubilities and Ostwald coefficients. Quantum mechanical and physical descriptors were calculated using HyperChem. A model describing the water solubility was then made from these descriptors and the measured water solubility by using Unscrambler. Prediction of the solubility of PFMCP gave an aqueous solubility of 6.89 × 10^{-6} [M] and an Ostwald coefficient of 3.445 × 10^{-4}. The value of the Ostwald coefficient for air used was 1.71 × 10^{-2}.

Acoustic bubble model

The inversion requires an accurate model of the interaction of bubbles with the incident sound field. A number of models for the propagation of non-linear pressure waves in bubbly liquids are available in the literature (Ainslie and Leighton 2011). Here we restrict measurements to the propagation of low-amplitude acoustic waves, which effectively places measurements in the linear region; hence a linear model is employed. We also restrict consideration and measurements to bubble

densities for which the Foldy (1945) approximation is applicable. Relevant theory is presented in Commander and Prosperetti (1989). The equations used are summarized in the following.

The complex sound speed, c_m, for sound propagation in a homogenous bubbly mixture is given by

$$\frac{c^2}{c_m^2} = 1+4\pi c^2 \int_0^\infty \frac{a\Psi(a)da}{\omega_0^2-\omega^2+2ib\omega} \tag{A17}$$

Here Ψ (a) is the bubble density and Ψ (a) da is the number of bubbles per unit volume with radius in the interval $(a, a + da)$. Formally there is also a time dependence associated with Ψ that we wish to measure. However, the function Ψ is considered independent of time during the time scale of a single measurement, and therefore, Ψ is modeled as time independent for the inversion of a single measurement set. Setting $c/c_m = u-iv$, the phase velocity, V, of the sound wave is

$$V = c/u \tag{A18}$$

and the intensity attenuation coefficient, α, in decibels per unit length, is given by

$$\alpha = 20(\log_{10}e)\,\omega v/c \tag{A19}$$

b is the total damping. The damping expressions used are

$$b = \frac{2\mu}{\rho a^2}+\frac{p_0}{2\rho a^2\omega}\mathrm{Im}\Phi+\frac{\omega^2 a}{2c} \tag{A20}$$

$$\Phi = \frac{3\gamma}{1-3(\gamma-1)i\chi\left[(i/\chi)^{1/2}\coth(i/\chi)^{1/2}-1\right]} \tag{A21}$$

$$\chi = D/\omega a^2 \tag{A22}$$

where D_g is the gas thermal diffusivity, γ is the ratio of specific heats, μ is the liquid viscosity and σ its surface tension. p_0 is the undisturbed pressure in the bubble given by $p_0 = p_\infty + 2\sigma/a$, and p_∞ is the equilibrium pressure in the liquid.

The resonance frequency, ω_0, is provided by

$$\omega_0^2 = \frac{p_0}{\rho a^2}\left(\mathrm{Re}\Phi-\frac{2\sigma}{ap_0}\right) \tag{A23}$$

The preceding model provides expressions for the principal acoustic properties of linear waves propagating in a bubbly medium and is relevant to a homogeneous population of free gas bubbles at low volume fraction.

Model limitations

The acoustic model used relies on the assumption for the case of radial motion of the bubble wall only. Other modes of vibration are not incorporated. This will not be as valid an assumption for "trapped" *in vivo* bubbles, but is reasonable for bubbles in the *in vitro* and extracorporeal measurement chambers. The possibility exists for non-linear coupling of activation fields and low-frequency pulse used for bubble sizing. However, experiments reveal that the acoustic sizing signal is unaffected by the presence or absence of the activation field for the experimental conditions imposed.

The specific constituents of the gas content of an activated bubble have not been directly measured and may vary with time. Thus, there may be some uncertainty in the exact value of γ. The bubble dynamics model requires values of the physical constants μ and σ. These values are not known exactly. At present the values for air and water or blood are used. The preceding model is for "clean" bubbles without a shell. Activated bubbles may be intrinsically "dirty" because of remnants of the contrast agent bubble and surfactant shells and accumulation of blood proteins at the blood gas interface, altering its resonance properties.

The applicability of the Foldy approximation will depend on the acoustic wave and bubble population. Commander and Prosperetti (1989) have reviewed the correspondence of the published data for linear waves in bubbly fluids with the accompanying theory. Correspondence deteriorates at volume fractions as low a $1e-4$, when the frequency of the wave is around the resonance frequency of the bubble population. This is attributed to the dramatic increase in scattering cross section around resonance. This resonant increase in interaction with the sound field effectively makes the void fraction "appear greater" to the acoustic wave than it actually is. The model will obviously fail if the average pressure field exciting the bubble is on the same order of magnitude or smaller than the scattered field from a neighboring bubble. This imposes the limitation

$$\left(a/d\right)\omega/\left|\omega_0^2-\omega^2+2ib\omega\right| \ll 1 \tag{A24}$$

where d is the distance between the bubbles. If this is quantified as the average inter-bubble distance $n^{-1/3}$, then the inequality may be expressed as $n^{2/3}\sigma_s \ll 1$. Other limits appear in the multiple scattering literature, such as, $n\sigma_s/k \ll 1$ (Waterman and Truell 1961), and $na\sigma_s^{1/2} \ll 1$ (Twerski 1962).

Table A1. Simulation parameter values

Parameter	*In vitro*	*Ex vivo*
τ	0.052 N/m	0.052 N/m
p_{atm}	101 kPa	101 kPa
p_{air}	85 kPa	98 kPa
p_{blood}	0 kPa	16* kPa
L_A	1.71×10^{-2}	1.71×10^{-2}
L_F	3.445×10^{-4}	3.445×10^{-4}
D_A	2.68×10^{-9} m^2/s	2.68×10^{-9} m^2/s
D_{pf}	9.62×0^{-10} m^2/s	9.62×10^{-10} m^2/s
X_{pf}	1	1

* 13.3 kPa average arterial pressure + 2.7 kPa as the cell is 25 cm below the cardiac chamber.

SYMBOLS

a	Bubble radius
d	Average inter-bubble distance
σ_s	Bubble scattering cross section
σ_e	Bubble extinction cross section
ω	Angular frequency
ω_0	Bubble resonance angular frequency
n	Number of bubbles per unit volume
D_g	Gas thermal diffusivity
k	Angular wavenumber
c_m	Complex sound speed in bubbly mixture
α	Intensity attenuation coefficient
V	Phase velocity
b	Damping constant
Ψ	Bubble number density
γ	Gas thermal diffusivity
μ	Liquid viscosity
σ	Surface tension
p_0	Pressure inside bubble
p_∞	Equilibrium liquid pressure
α (f)	Frequency-dependent attenuation function
B_j (a)	jth linear B spline
β_j	Volume fraction
dc_j'	Predicted sound speed anomaly
dc_j''	Measured sound speed anomaly
Δc_j	Difference between dc_j' and dc_j''

V_g Volume of gas
v_{pf} Volume of pf-MCP liquid
p_{pf} Partial pressure of PFMCP vapor
p_{air} Partial pressure of air
p_{atm} Atmospheric pressure
p_{blood} Systemic blood pressure
ρ_{pf} Mass density of PFMCP, 1.7×10^3 kg/m^3 for PFMCP
mw_{pf} Molecular weight of PFMCP
N_a Avogadro's number
k_b Boltzmann constant
T Temperature
D_b Diameter of gas bubble
D_d Diameter of liquid droplet
D_{pf}, D_A Diffusion coefficients of pf-MCP and air, respectively
L_{pf}, L_A Ostwald coefficients of pf-MCP and air respectively
τ Surface tension
P_w Pressure in the surrounding fluid phase
p_w Partial pressure of all gases in the surrounding fluid phase
R Gas constant
t Time
C_A, C_{pf} Concentrations of air and pf-MCP, respectively
c_A, c_{pf} Concentrations of air and pf-MCP in liquid, respectively
J_{pf} Steady-state diffusional flux of pf-MCP
r_0 Bubble radius at time 0
$\mu = \frac{2\tau}{p_{atm} r_0}$ Dimensionless Laplace pressure
$\vartheta = \frac{p_{blood}}{p_{atm}}$ Dimensionless systemic pressure
$\rho = \frac{r}{r_0}$ Dimensionless radius
$\delta = \frac{D_A}{D_{pf}}$ Ratio of diffusion coefficients
$\chi_A = \frac{C_A RT}{p_{atm}}$ Dimensionless concentration of air in the bubble
$\chi_{pf} = \frac{C_{pf} RT}{p_{atm}}$ Dimensionless concentration of pf-MCP in the bubble
$\Gamma = \frac{D_{pf}}{r_0^2} t$ Dimensionless time
$F = \chi_{pf} \rho^3$ Parameter
$A = \chi_A \rho^3$ Parameter
$p_d = \frac{p_{air}}{p_{atm}}$ Dimensionless relative air partial pressure
X_{fp} Mole fraction of pf-MCP at $t = 0$